Atmos. Chem. Phys., 26, 11067–11089, 2026
https://doi.org/10.5194/acp-26-11067-2026

Atmospheric Chemistry and Physics
Open Access
EGU

Research article

Molecular characteristics and formation pathways of organosulfur compounds: a comparative field study across contrasting atmospheric environments

Dongmei Cai[1,2,3], Xianda Gong[1,2], Runqi Zhang[3], Shenyan Zhang[4], Yuhan Cheng[1,2], Saidur Rahaman[1,2], Yin Fang[4], and Jianmin Chen[3]

[1]Key Laboratory of Coastal Environment and Resources of Zhejiang Province, School of Engineering, Westlake University, Hangzhou, Zhejiang 310030, China
[2]Research Center for Industries of the Future, Westlake University, Hangzhou, Zhejiang 310030, China
[3]Shanghai Key Laboratory of Atmospheric Particle Pollution and Prevention (LAP3), IRDR ICoE on Risk Interconnectivity and Governance on Weather/Climate Extremes Impact and Public Health, Department of Environmental Science and Engineering, Fudan University, Shanghai 200438, China
[4]State Key Laboratory of Estuarine and Coastal Research, Institute of Eco-Chongming, Blue Carbon Science and Technology Centre, East China Normal University, Shanghai, 200241, China

Correspondence: Xianda Gong (gongxianda@westlake.edu.cn) and Jianmin Chen (jmchen@fudan.edu.cn)

Received: 29 April 2026 – Discussion started: 13 May 2026
Revised: 28 July 2026 – Accepted: 29 July 2026 – Published: 7 August 2026

Abstract. Organosulfur compounds (OrgSs), especially organosulfates (OSs), are ubiquitous aerosol components. However, the spatial, seasonal, and day-night variations of OrgS formation in polluted atmospheres remain poorly understood. Here, we monitored particulate OrgSs at an urban site and a suburban site in Shanghai and investigated their molecular composition and potential formation pathways under contrasting atmospheric conditions. A total of 1964, 1914, and 2689 OrgS molecular formulas were detected in suburban summer, urban summer, and urban winter, respectively. More than 79 % of sulfur-containing molecular formulas satisfied $(4s + 3n)/o \leq 1$, indicating that the detected OrgS species were predominantly potential OSs and nitrooxy-OSs (NOSs). Compared with summer, wintertime OrgSs exhibited lower O/C ratios but higher double-bond equivalence and aromaticity, suggesting a stronger influence of anthropogenic emissions and more unsaturated molecular structures. Although OrgSs were mostly present in aliphatic molecular structures, an increase in the number of aromatic OSs in winter revealed an enhanced contribution from anthropogenic sources. Isoprene/monoterpene-derived OSs peaked during the daytime in summer, whereas monoterpene-derived NOSs were markedly enhanced at night, consistent with daytime photochemistry and nighttime NO_3-initiated oxidation, respectively. Non-metric multidimensional scaling analysis further revealed that OrgS composition in summer was associated with temperature and O_3 during the day but shifted toward RH-driven processing at night. In winter, inorganic nitrogen and sulfur species, aerosol liquid water content, and particle acidity became more important in shaping OrgS composition, highlighting the potential importance of multiphase and acid-catalyzed formation. These findings provide molecular-level insights into the sources and formation of atmospheric OrgSs across contrasting environments.

Published by Copernicus Publications on behalf of the European Geosciences Union.

1 Introduction

Organosulfur compounds (OrgSs) are ubiquitous in the atmosphere, spanning diverse environments from remote regions to highly polluted urban areas (Cai et al., 2020; Zhang et al., 2025; Yang et al., 2024; Thomas et al., 2025). They have been recognized as an important component in ambient $PM_{2.5}$ (up to 50 %) (Surratt et al., 2008; Tolocka and Turpin, 2012; Lukács et al., 2009), and have critical influences on aerosol physicochemical properties, such as acidity, hygroscopicity, and volatility (Hansen et al., 2015; Fan et al., 2022). OrgSs exhibit notable chemical stability and environmental persistence, including organosulfates (OSs), sulfoxides, sulfonates, and sulfones, among which OSs have been identified as the most abundant class (Cai et al., 2020; Wang et al., 2018b; Jiang et al., 2022). Emerging evidence has underscored the hygroscopicity, light absorption, and potential toxicity of OSs (Jiang et al., 2025; Hansen et al., 2015; Fan et al., 2022), further highlighting the critical need for in-depth investigations into the composition, sources, and formation pathways of atmospheric OrgSs.

Although OrgSs can be directly emitted from the combustion of fossil fuels and biomass, they are mainly formed through heterogeneous or multiphase reactions of sulfur dioxide (SO_2) and sulfate particles with anthropogenic and biogenic volatile organic compounds (BVOCs) (Brüggemann et al., 2020b; Tang et al., 2020). The acid-catalyzed ring-opening of epoxides in the presence of sulfuric acid seeds has been widely invoked to explain OS formation (Jiang et al., 2022; Cai et al., 2020). Additionally, OSs may be formed by sulfate radical-induced oxidation of unsaturated compounds (Schindelka et al., 2013; Noziere et al., 2010), nucleophilic substitution of tertiary organonitrates with sulfate (Darer et al., 2011), and sulfate esterification of alcohols or epoxides (Minerath et al., 2008; Minerath and Elrod, 2009). Direct formation of OSs from uptake of gaseous SO_2 by unsaturated fatty acids and organic peroxides (Shang et al., 2016; Ye et al., 2018), as well as from reactions between sulfite/sulfate ion radicals and unsaturated carbonyl compounds in the presence of Fe^{3+}, have also been reported (Huang et al., 2018). Furthermore, nighttime NO_3-initiated oxidation of BVOCs is recognized as a crucial formation pathway of nitrooxy-organosulfates (NOSs) (Hamilton et al., 2021; Surratt et al., 2008; Wang et al., 2018b). The presently proposed formation pathways presumably explain the large variety and ubiquity of OSs. However, the chemical composition of OrgSs in the actual atmosphere is highly complex, and the atmospheric relevance of these processes has yet to be fully elucidated.

The formation of OSs is strongly influenced by anthropogenic sulfate, NO_x, BVOCs, and ambient conditions, such as, relative humidity (RH) and aerosol physical properties. As these factors vary across different atmospheric environments, field observations are indispensable for validating mechanistic insights from chamber experiments and uncovering previously unrecognized environmental factors. Shanghai, a coastal megacity in the Yangtze River Delta (YRD) region of China, provides a unique environment for investigating the formation and evolution of particulate OrgSs because its atmospheric environment is shaped by strong local emissions, regional transport, and pronounced seasonal meteorological contrasts. This region is characterized by high emissions of VOCs and gaseous pollutants (e.g., NO_x and SO_2), together with generally high RH and strong oxidizing capacity, which can foster complex biogenic-anthropogenic interactions (Cai et al., 2020; Yang et al., 2023; Han et al., 2023b). Furthermore, urban and suburban environments differ in emission intensity and precursor composition. These spatial and seasonal contrasts create favorable conditions for examining how anthropogenic–biogenic interactions regulate OrgS formation. Although several studies have reported the concentrations and potential formation mechanisms of biogenic VOC-derived OSs in the YRD, these OSs represented only a small fraction of total particulate OrgSs in ambient aerosols (Yang et al., 2023; Wang et al., 2021b). Therefore, a better understanding of the molecular characteristics, formation mechanisms, and key influencing factors of OrgSs in Shanghai is crucial for elucidating their role in particulate pollution and developing effective strategies to mitigate secondary organic aerosol (SOA) concentrations.

In this study, we used ultra-high performance liquid chromatography coupled with an Orbitrap mass spectrometer (UHPLC-Orbitrap MS) to characterize particulate OrgSs in Shanghai, based on field campaigns conducted at a suburban site in summer and at an urban site in both summer and winter. This strategic sampling captures the spatial, seasonal, and day-night variability of OrgSs under contrasting atmospheric conditions. Our main objective was to unravel the spatiotemporal evolution, potential formation pathways, and key drivers of OrgSs at the molecular level, by comparing their compositional and structural characteristics across summer versus winter, day versus night, and low versus high sulfate and NO_x levels. This work provides molecular-level insights into organosulfur chemistry and is pivotal for assessing the role of anthropogenic pollutants in driving SOA formation in biogenically influenced urban regions.

2 Materials and methods

2.1 Aerosol sampling and site description

Ambient $PM_{2.5}$ sampling was conducted in both the urban center of Shanghai (Fudan University, Yangpu Jiangwan Campus; 31.344° N, 121.518° E) and a suburban area (Qingpu Dianshan Lake; 31.136° N, 121.092° E). The urban site is representative of typical urban environments, characterized by high population density and heavy traffic emissions. The suburban site, located approximately 62 km northeast of the urban site, is influenced by a mix of regional pollutant transport and local biogenic emissions. Sampling cam-

paigns were carried out during summer (22 July to 2 August 2023) and winter (9 to 20 January 2024) at the urban site, and during summer (18 July to 2 August 2023) at the suburban site. Sampling was conducted separately during daytime (07:00–18:30, local time, UTC+8) and nighttime (19:00–06:30) to capture the day-night variations in the formation of OrgSs. It should be noted that winter samples were available only at the urban site; therefore, the seasonal comparison in this study is restricted to the urban campaign, whereas the urban-suburban comparison is discussed only for the summer period. All $PM_{2.5}$ samples were collected onto pre-baked quartz fiber filters (Whatman Inc.) using high-volume samplers (TH-1000C, Tianhong, China) at a flow rate of 1.05 m^3 min^{-1}. Additionally, 11.5 h field blank samples were also collected by turning off the sampling pump. A total of 48 $PM_{2.5}$ samples and 4 field blank samples were obtained from the urban site, while 32 $PM_{2.5}$ samples and 2 field blank samples were collected from the suburban site. All filter samples were stored at −20 °C before analysis. The real-time monitoring of O_3, NO, NO_2, and meteorological parameters was also conducted during each sampling campaign (Table S1 in the Supplement).

2.2 Chemical analysis and prediction of aerosol acidity and ALW

A 24 cm^2 aliquot was excised from each $PM_{2.5}$ filter sample and subjected to ultrasonic extraction three times, each with 3 mL of methanol for 30 min. The combined extracts were filtered through a 0.45 µm PTFE syringe filter to remove insoluble particles, then concentrated to near dryness under a gentle stream of nitrogen. The residue was reconstituted in 80 µL of methanol containing internal standards (IS, 200 ppb D_{17}-Octyl sulfate). The resulting solution was centrifuged at 10 000 rpm for 10 min, and the supernatant was collected for subsequent mass spectrometry analysis.

Sample extracts were analyzed using an ultra-high performance liquid chromatography system coupled with an Orbitrap Exploris 120 mass spectrometer (UHPLC-Orbitrap MS, Thermo Scientific, Germany). The electrospray ionization source was operated in negative ionization mode with the following settings: capillary temperature of 320 °C, auxiliary gas flow at 10 units, sheath gas flow at 35 units, sweep gas flow at 2 units, and spray voltage at 3.0 kV. The scan range was m/z 60–900, with a resolution of 120 000 at m/z 200. Chromatographic separation was performed on an Acquity UPLC HSS T3 column (1.8 µm, 100 mm × 2.1 mm, Waters) with a C18 guard column (HSS T3, 1.8 µm). The flow rate was set to 0.3 mL min^{-1}, the column temperature was maintained at 40 °C, and the injection volume was 5 µL. The mobile phase used a binary gradient, with solvent A as 0.1 % formic acid in water and solvent B as 0.1 % formic acid in acetonitrile. The gradient program was as follows: 10 % B was held for 2 min, linearly increased to 30 % B over 2–25 min, further increased to 90 % B over 25–50 min, held at 90 % B for 10 min (50–60 min), then decreased to 10 % B over 60–61 min, followed by a 9 min column re-equilibration at 10 % B prior to the next injection. External mass calibration was performed every 3 d using a commercial calibration solution (Ultramark 1621, Thermo Fisher, Germany) covering an m/z range of 74–1922. Due to the limited volume of the final extract (80 µL), duplicate injections were not performed. Instead, the remaining sample solution from the first injection was retained for potential targeted analyses rather than systematic re-injection. All chromatographic peaks exhibited typical Gaussian shapes, indicating satisfactory column performance and separation efficiency. Field blank samples were extracted and analyzed following the same procedure to account for potential background contamination.

Organic carbon (OC) and elemental carbon (EC) were determined using a thermal/optical carbon analyzer (DRI model 2001, Desert Research Institute, USA) with the well-established IMPROVE-A thermal/optical reflectance protocol. Organic matter (OM) was calculated by multiplying the OC by 1.6 (Liu et al., 2018; Xing et al., 2013; Turpin and Lim, 2001). Water-soluble inorganic ions (e.g., SO_4^{2-}, NO_3^-, Cl^-, NH_4^+, K^+, Na^+, Ca^{2+}, and Mg^{2+}) were quantified by an ion chromatograph (940 Professional IC Vario, Metrohm) following procedures described by Cai et al. (2020).

The aerosol liquid water content (ALWC) and acidity (pH) were calculated using the ISORROPIA-II thermodynamic model. ISORROPIA-II was run in forward mode, assuming the particles were in a "metastable" state. The input parameters included environmental relative humidity (RH), temperature (T), and the inorganic components of the particle phase (SO_4^{2-}, NO_3^-, Cl^-, NH_4^+, K^+, Na^+, Ca^{2+}, and Mg^{2+}) (Hennigan et al., 2015; Weber et al., 2016; Guo et al., 2015; Song et al., 2018b). Gaseous NH_3, measured by an ammonia analyzer (G2103, Picarro, California, USA), was taken into consideration in the model during the summertime and wintertime campaigns at the urban site. The simulated NH_3 concentrations agreed well with the observations (Fig. S1a). Due to the lack of gaseous NH_3 data at the suburban site, an iteration-based method was applied to reduce potential underestimation of aerosol pH (He et al., 2025; Li et al., 2024b). Only measured aerosol NH_4^+ was used as the total ammonia input for the first run. The predicted gaseous NH_3 from each run was then added to the original NH_4^+ concentration to update the total ammonia input for the subsequent run. The sixth iteration produced the closest outcome to pH values constrained by observed NH_3 and was therefore adopted for suburban-site calculations (Fig. S1b, c). At the suburban site, the variance in the predicted NH_4^+ mass concentrations between successive iterations fell below a threshold of 0.01 by the sixth iteration, supporting the convergence and applicability of the iterative approach. Moreover, significant correlations between the results of the first run and the sixth run were observed for pH ($R^2 = 0.95$) and ALWC ($R^2 = 0.99$, Fig. S1), further indicating the stability and reliability in estimating the pH and ALWC by ISORROPIA II.

2.3 Data processing and statistical analysis

Raw data were acquired using Xcalibur software (V2.2; Thermo Scientific). The HPLC-HRMS data were processed with MZmine-2.33 software (http://mzmine.github.io, last access: 3 April 2026) to obtain the m/z ratios, formulas, retention times, and peak areas of detected organic compounds (Wang et al., 2017; Hu et al., 2016; Cai et al., 2024). The molecular formula assignment was mainly based on detected m/z values with a mass tolerance of ±2 ppm. The compounds assigned as $C_{1–40}H_{1–100}O_{1–20}N_{0–4}S_{0–2}$ with $s = 1$ or 2 will be collectively referred to as organosulfur compounds, including CHOS ($n = 0$) and CHONS ($n = 1$ or 2).

For chemical formula $C_cH_hO_oN_nS_s$, the double bond equivalent (DBE) value, representing the degree of unsaturation, can be calculated by Eq. (1):

$$\mathrm{DBE} = \frac{(2c + 2 + n - h)}{2} \tag{1}$$

The aromaticity equivalent (X_c) was introduced by Yassine et al. (2014) for the identification and characterization of monocyclic and polycyclic aromatic compounds. The X_c for compounds containing only carbon, hydrogen, nitrogen, oxygen, and sulfur can be calculated following Eq. (2):

$$X_c = \frac{3\left[\mathrm{DBE} - (i \times o + j \times s)\right] - 2}{\mathrm{DBE} - (i \times o + j \times s)} \tag{2}$$

where i and j correspond to the fractions of oxygen and sulfur atoms involved in the π-bond structures of a compound, respectively. Here, $i = j = 0.5$ was applied for the calculation of X_c values of compounds detected in ESI-, as carboxylic compounds with $p = q = 0.5$ are preferably ionized in negative mode (Tong et al., 2016; Wang et al., 2017). If $\mathrm{DBE} \le i \times o + j \times s$, then X_c was defined as zero. The ranges of $2.50 \le X_c < 2.71$, $2.71 \le X_c < 2.80$, $2.80 \le X_c < 2.83$, and $2.83 \le X_c$ are proposed as unambiguous minimum criteria for the presence of mono-, di-, tri-, and polycyclic aromatics, respectively (Yassine et al., 2014).

Given the large number of detected OrgSs, it is impractical to evaluate the ionization efficiencies of each compound. In this study, qualitatively comparing the variation trends of different compounds detected by HR-MS is a commonly used and valid approach for characterizing the overall molecular composition of OA across different sites or seasons (Zhang et al., 2024; Wang et al., 2024b; Cai et al., 2020). Accordingly, despite the potential influence of matrix effects, analyzing and comparing the number or signal intensity percentages of different OrgS categories can, to some extent, reflect the variability in the molecular composition of OrgSs under varying atmospheric conditions. To further assess the impact of matrix effects in different samples, we spiked all samples with 200 ppb of D_{17}-Octyl sulfate as an internal standard (IS). The IS intensity exhibited minimal variability across different samples, indicating that matrix effects on ionization efficiency can be considered negligible. The abundance of each compound refers to its chromatographic peak area, and all detected abundances were blank-corrected. To facilitate more accurate comparisons, the relative abundance of each OrgS compound was defined as the ratio of its blank-corrected peak area to that of IS (set as 100 %) within the same sample. We note that the OrgS results reported here are based on IS-normalized peak areas rather than absolute mass concentrations. Because authentic standards are unavailable for most OrgS species and ESI response factors vary among different molecular structures, the present non-target dataset is mainly suitable for comparing molecular composition and relative abundance patterns, rather than for direct concentration-based comparison with other studies and model evaluations. Future work using authentic standards or improved semi-quantitative approaches is needed to better constrain the absolute concentrations of OrgS species and facilitate direct comparison with model outputs.

To evaluate the associations between environmental variables and OrgSs in suburban summer, urban summer, and urban winter, nonmetric multidimensional scaling (NMDS) analysis was conducted based on Bray–Curtis distances in R using the vegan package (Jiang et al., 2022). For all three sample sets, the OrgS compounds were dimensionally reduced to two components (NMDS1 and NMDS2), and all stress values were less than 0.15. The selected environmental parameters, including meteorological parameters (T and RH), gaseous pollutants (NO_2, CO, SO_2, O_3, and NO), chemical tracers (EC, K^+, and Cl^-), inorganic nitrogen and sulfur species (SO_4^{2-}, NO_3^-, and NH_4^+) as well as ALWC and pH, were fitted onto the ordination plot to evaluate the key environmental drivers influencing the molecular distributions of OrgSs. The significance (p-values) of the correlations between the environmental parameters and the NMDS dimensions was assessed using 999 permutations. Only the factors significantly correlated with the NMDS dimensions were reserved and could be considered as the possible drivers associated with molecular distribution. Score and loading plots were constructed according to NMDS variables from each OrgSs compound (gray triangles and circles). The potential driving factors associated with the molecular distribution of OrgSs were indicated by arrows, with their direction and angle representing the relationship between the variables and each dimension. Spearman correlation between the sum-normalized peak areas of individual molecules and some important environmental variables and chemical tracers was performed in R, and then VK diagrams were plotted for each variable based on the Spearman correlation coefficients (Kellerman et al., 2014). Molecules found in at least four samples were adopted for correlation analysis. A false discovery rate-adjusted p-value was applied to avoid errors arising from using a large dataset.

2.4 Molecular Corridors and Parameterizations of Volatility

Accurate prediction of volatility is primarily based on the structural information of the organic compounds; however, it is often difficult to obtain from field measurements. Li et al. (2016) predicted C_0 as a function of elemental composition that is often determined by soft – ionization high – resolution mass spectrometry (Wang et al., 2024b; Xie et al., 2021, 2020). The parameter of $\log_{10}C_0 = f(c, o, n, s)$ to be applicable to the sulfur–containing compounds can be calculated as shown in Eq. (3):

$$\log_{10}C_0 = \left(n_C^0 - n_C\right)b_C - n_O b_O - 2\frac{n_C n_O}{n_C + n_O}b_{CO} - n_N b_N - n_S b_S \quad (3)$$

where n_C^0 is the reference carbon number; n_C, n_O, n_N, and n_S denote the numbers of carbon, oxygen, nitrogen, and sulfur atoms, respectively; b_C, b_O, b_N, and b_S denote the contribution of each atom to $\log_{10}C_0$, respectively; and b_{CO} is the carbon-oxygen nonideality (Donahue et al., 2011). According to the values of C_0, OrgSs can be classified as (1) volatile organic compounds (VOC; $C_0 > 3\times 10^6\,\mu g\,m^{-3}$), (2) intermediate volatility OC (IVOC; $300 < C_0 < 3\times 10^6\,\mu g\,m^{-3}$), (3) semivolatile OC (SVOC; $0.3 < C_0 < 300\,\mu g\,m^{-3}$), (4) low-volatile OC (LVOC; $3\times 10^{-4} < C_0 < 0.3\,\mu g\,m^{-3}$), and (5) extremely low-volatile organic compounds (ELVOC; $C_0 < 3\times 10^{-4}\,\mu g\,m^{-3}$) (Donahue et al., 2011; Murphy et al., 2014). The peak area-weighted average $\log_{10}C_0$ can be calculated as

$$\log_{10}C_{0\text{avg}} = \frac{\sum\left(\log_{10}C_{0i}\times A_i\right)}{\sum A_i} \quad (4)$$

Here, A_i is the peak area for each individual compound i.

3 Results and discussion

3.1 Molecular Characteristics of OrgSs

By using UHPLC-Orbitrap MS analysis, a total of 1964, 1914, and 2689 organosulfur formulas were detected in suburban summer, urban summer, and urban winter aerosol samples, respectively. The intensity and number of detected particulate-phase OrgSs were significantly higher in winter than in summer, which aligns with the seasonal variations in $PM_{2.5}$ and OM concentrations (Table S1). Nevertheless, the comparable OM-normalized OrgS intensities (OrgS / OM ratios) between urban summer and winter (Fig. S2) indicate that the elevated OrgS intensity in winter largely accompanied the increase in bulk OM rather than reflecting preferential enrichment of OrgSs. Accordingly, the larger number of formulas detected in winter may may partly result from higher OM loading and associated detection-threshold effects. Moreover, formula-based volatility analysis showed that the relative peak area-weighted contribution of SVOC to total OrgSs increased from 37 % in summer to 41 % in winter (Fig. S3), consistent with the enhanced partitioning of semivolatile OrgSs into the particle phase at lower temperatures (Huang et al., 2019). Further class-specific analysis revealed that the SVOC contribution to CHOS increased from 47 % in summer to 54 % in winter, whereas the ELVOC contribution to CHONS increased from 81 % in summer to 90 % in winter. This increased relative importance of low-volatility CHONS may also be associated with seasonal variations in precursor sources and atmospheric chemical processing. Overall, these results suggest that the wintertime particle-phase OrgS composition may be partly influenced by temperature-dependent gas–particle partitioning and seasonal variations in sources and chemical processing (Li et al., 2016; Xie et al., 2021). Because only particle-phase samples were analyzed, the relative contributions of chemical formation versus gas-particle partitioning could not be quantitatively distinguished.

The identified OrgSs can be classified into six categories: $CHOS_1$, $CHOS_2$, $CHON_1S_1$, $CHON_1S_2$, $CHON_2S_1$, and $CHON_2S_2$. $CHOS_1$ and $CHON_{1\text{–}2}S_1$ account for ∼ 88 % of the molecular number and ∼ 96 % of the total intensity of OrgSs (Table S3), suggesting their dominant roles in OrgS composition. Notably, the intensity contribution of $CHOS_1$ in suburban summer was lower than those in urban summer and winter, whereas $CHON_{1\text{–}2}S_1$ showed an opposite trend. This disparity underscores the distinct influences of geographical location and seasonality on OrgS composition, as discussed in detail below. Furthermore, as many as 79 %–92 % of OrgS species contained enough oxygen atoms to enable the assignment of $-OSO_3H$ and $-ONO_2$ groups (e.g., $(4s+3n)/o \leq 1$) in their formulas, suggesting that they were potential OSs or nitrooxy-OSs (NOSs), which is consistent with previous studies (Cai et al., 2020; Wang et al., 2016). However, this formula-based criterion provides only a tentative classification and does not constitute unambiguous structural confirmation. For compounds with available MS/MS spectra, OS / NOS assignments were further conducted based on diagnostic sulfate- and nitrate-related fragment ions (e.g., $SO_3^{\bullet-}$ m/z 79.9574, HSO_3^- m/z 80.9652, HSO_4^- m/z 96.9601, and NO_3^- m/z 61.9884) (Hettiyadura et al., 2015; Riva et al., 2016b). Specifically, OSs were selected based on compounds with $O/S \geq 4$ and HSO_4^- (m/z 96.9601) or HSO_3^- (m/z 80.9652) fragments observed in their corresponding MS/MS spectra (Figs. S4, S5), whereas CHONS species satisfying $(4s+3n)/o \leq 1$ and exhibiting both NO_3^- (m/z 61.9884) and $SO_3^{\bullet-}$ (m/z 79.9574) fragments were defined as NOSs (Figs. S6). These compounds subjected to MS/MS analysis accounted for more than 50 % of the total intensity of all potential OSs / NOSs (Table S2). It should be noted that many low-abundance CHOS and CHONS species could not trigger reliable data-dependent MS/MS acquisition and were therefore classified as potential OSs or NOSs based solely on elemental com-

position, potentially leading to an overestimation of the total OS / NOS intensity.

3.1.1 CHOS species

CHOS species predominated in both suburban and urban samples, accounting for 65 %–77 % of the total OrgS intensity (Table S3). The majority (83 %–88 %) of CHOS formulas were assigned with $4s/o \leq 1$, suggesting that these compounds are potential OSs (Lin et al., 2012b). Clear seasonal differences were observed in their molecular characteristics. In urban samples, CHOS species in summer exhibited higher O/C_w and H/C_w ratios ($O/C_w = 0.53 \pm 0.11$, $H/C_w = 1.81 \pm 0.04$) than those in winter ($O/C_w = 0.45 \pm 0.06$, $H/C_w = 1.62 \pm 0.03$), whereas the average DBE_w of wintertime CHOS compounds (2.56 ± 0.47) exceeded that in summer (2.18 ± 0.44). These results indicate that wintertime CHOS species were characterized by the lower oxidation state and higher unsaturation degree and aromaticity, likely associated with intensified anthropogenic emissions in winter and enhanced photochemical processing in summer. The enhanced anthropogenic influence in winter can be further supported by the aromaticity equivalent (X_c), a parameter determining the presence of monoaromatics ($X_c \geq 2.50$) and polyaromatics ($X_c \geq 2.71$) (Yassine et al., 2014). As depicted in Fig. 1b, c, f, the intensity fraction of CHOS compounds with $X_c \geq 2.5$ was greater in winter (18 % ± 8 %) than in urban summer (10 % ± 5 %). Aromatic CHOS compounds were dominated by phenyl OrgSs with $2.50 \leq X_c < 2.71$, accounting for 70 % ± 14 % and 73 % ± 9 % of the total aromatic CHOS peak intensity in summer and winter, respectively, which possibly suggests significant influences from primary anthropogenic emissions (Cui et al., 2019; Song et al., 2018a; Ma et al., 2014). Furthermore, the intensity fraction of polyaromatic CHOS compounds ($X_c \geq 2.71$) increased from summer (3 % ± 2 % in urban) to winter (5 % ± 2 %), suggesting enhanced combustion emission during the cold season. This interpretation is consistent with the nearly twofold higher concentrations of combustion-related tracers (e.g., EC and CO) in winter than in summer. In contrast, higher temperatures and O_3 levels in summer likely facilitated stronger biogenic VOC emissions and more intense photochemical oxidation. All of those highlight seasonal differences in emission sources and secondary transformation processes of CHOS species in urban Shanghai.

Compared with urban summer, CHOS species in suburban summer exhibited slightly higher average O/C_w (0.58 ± 0.14) and H/C_w (1.88 ± 0.06) ratios, and a lower DBE_w value (2.06 ± 0.46), indicating a relatively higher degree of oxygenation and saturation in suburban CHOS species. Correspondingly, the intensity fractions of phenyl CHOS and polyaromatic CHOS in suburban summer were 7 % ± 5 % and 2 % ± 1 %, respectively, both slightly lower than those in urban summer. This spatial disparity is consistent with the weaker anthropogenic influence at the suburban site, where the average concentrations of EC and CO were approximately half of those observed at the urban site (Table S1). Conversely, the higher average O_3 level at the suburban site suggests stronger oxidative processing. These results imply that suburban CHOS composition was more strongly influenced by the oxidation of biogenic VOCs under summer conditions. Regionally, the H/C_w ratios of CHOS in this study were comparable to or exceeded those reported for ambient aerosols from diverse locations worldwide (Table S4) (Wang et al., 2024a; O'Brien et al., 2014; Jiang et al., 2022; Ning et al., 2025; Willoughby et al., 2014; Lin et al., 2012a; Rincón et al., 2012), suggesting that the OrgSs in Shanghai are relatively enriched with saturated structures. However, the O/C_w ratios of CHOS compounds identified in this study were slightly higher than that reported for $PM_{2.5}$ in Anshan (0.45) (Ning et al., 2025) and comparable to values measured in the Pearl River Delta (0.52 ± 0.07) (Jiang et al., 2022), but markedly lower than those reported for aerosols from California (0.82–0.93) and polluted organic aerosols from Mainz (0.78–1.44) and Chinese (1.17–1.48) cities (Wang et al., 2018a; O'Brien et al., 2014; Wang et al., 2021a; Wang et al., 2019). The differences identified in these comparisons may reflect regional variations in source emissions and subsequent atmospheric oxidation processes. Owing to spatiotemporal heterogeneity, the molecular characteristics of CHOS in Shanghai may differ from those reported in some regions, highlighting the need for further investigations into the sources and molecular-level distributions of atmospheric OrgSs. The most abundant class of CHOS species identified in all samples had 4–7 O atoms, with S_1O_5 being the most prevalent (Figs. 1d and S7a). This characteristic was most evident in the urban winter samples. The elevated oxygen content implies the presence of additional oxidized functional groups, such as hydroxyl and carbonyl. As shown in Fig. 1a–c, the main distribution of CHOS compounds falls within a DBE range of 1 to 10 and a carbon number range of 2 to 22. Based on established DBE classifications (Jiang et al., 2022; Lin et al., 2012b), the detected CHOS species were tentatively classified into three categories: saturated aliphatic-derived species ($DBE \leq 1$; 51 % ± 10 %), biogenic-derived species ($DBE = 2/3$; 23 % ± 12 %), and aromatic-derived species ($DBE \geq 4$; 26 % ± 15 %), collectively accounting for the total intensity of assigned CHOS compounds (Fig. 1e). CHOS compounds with $DBE \leq 3$ predominantly contained 8 to 22 carbon atoms, accounting for 59 % ± 13 % of the total CHOS intensity. The C_8–C_{22} compounds are likely associated with the oxidation products of monoterpenes (C_{10}) and sesquiterpenes (C_{15}), as well as dimeric and trimeric BVOC oxidation products (Daellenbach et al., 2019; Kourtchev et al., 2016). However, anthropogenic sources have also been proposed for C_8–C_{22} CHOS compounds, including the photooxidation of long-chain alkanes from vehicle emissions (Tao et al., 2014; Riva et al., 2016b) and heterogeneous reaction between SO_2

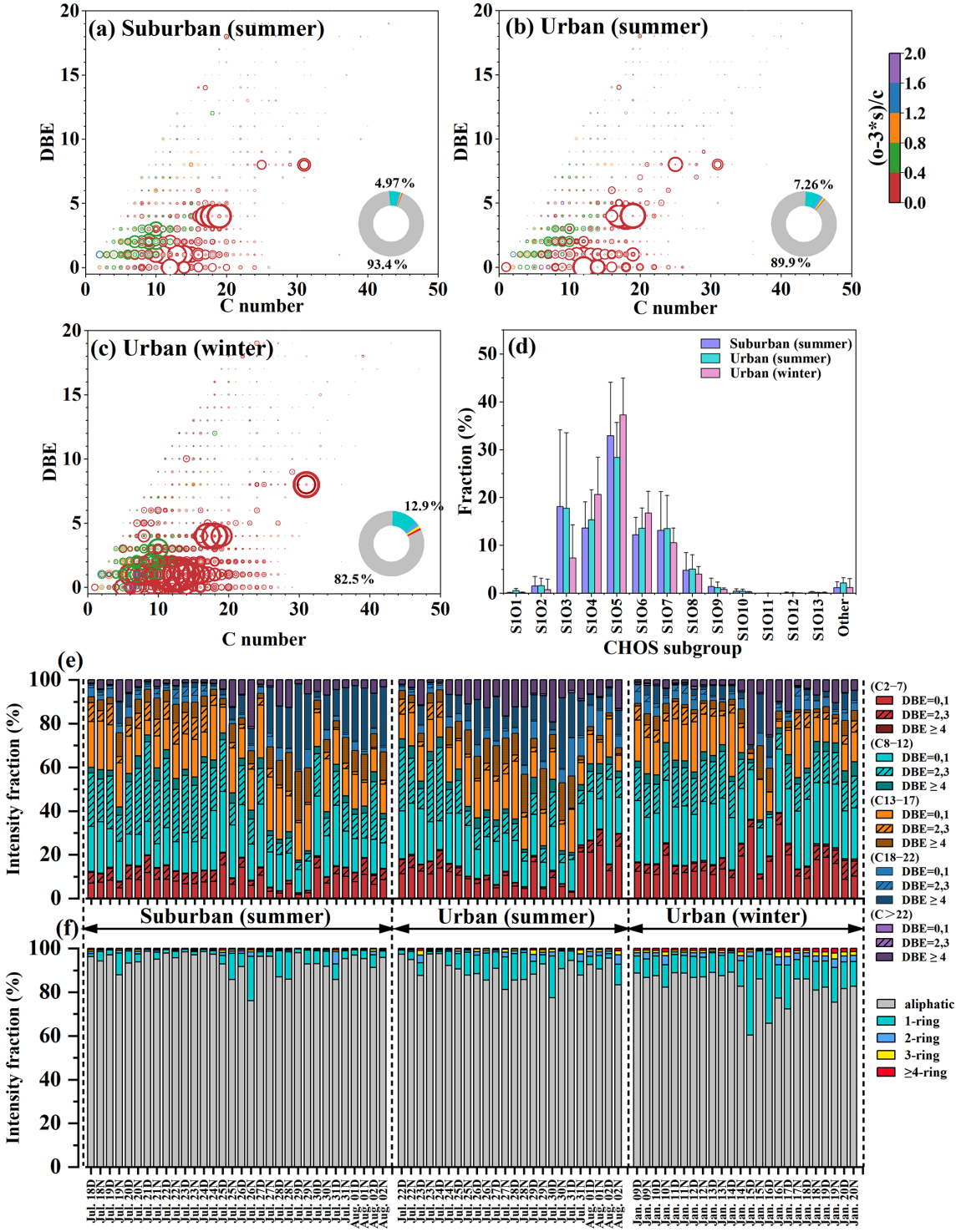

Figure 1. Molecular distribution of CHOS compounds detected by Orbitrap MS for the $PM_{2.5}$ samples collected in the three field campaigns. **(a–c)** Double-bond equivalent (DBE) vs. C number for all the CHONS compounds in the suburban (summer) and urban (summer, winter). The circle area is proportional to the square root of the relative abundance of individual molecules, and the color bar denotes the degree of oxidation. **(d)** Classification of CHOS species into different subgroups according to the numbers of S and O atoms in their molecules. **(e)** Percentages of the intensity of each subgroup divided based on the DBE value and the length of carbon skeleton in the formulas. **(f)** Intensity percentages of each subgroup which were divided based on the X_c value of formulas.

and unsaturated fatty acids in ambient particles (Zhu et al., 2019; Shang et al., 2016). For example, $C_{10}H_{18}O_6S$ and $C_{10}H_{18}O_7S$ could be formed via photooxidation of both biogenic (α-pinene) and anthropogenic (cyclodecane) precursors (Surratt et al., 2008; Riva et al., 2016b). These findings underscore the challenge of unambiguous source apportionment based solely on molecular formula. In addition to the dominant C_8–C_{22} compounds, low molecular weight CHOS compounds (C_2–C_7) with DBE ≤ 3 were also observed, which are likely isoprene derivatives or fragmentation products generated during atmospheric oxidation processes (Hatch et al., 2011; Riva et al., 2016a). High molecular weight compounds (C > 22) contributed minimally to the total CHOS signal. Among the CHOS compounds, five species (e.g., $C_9H_{16}O_7S$, $C_{10}H_{20}O_5S$, $C_{12}H_{26}O_4S$, $C_{14}H_{28}O_5S$, and $C_{16}H_{34}O_5S$) were identified as the dominant components in OA. $C_9H_{16}O_7S$ has been proposed to be mainly derived from the photooxidation of limonene/limonaketone in the presence of acidified sulfate seed aerosol (Surratt et al., 2008). The remaining four species, characterized by saturated aliphatic structures with DBE ≤ 1, suggest that their formation likely involves atmospheric oxidation and subsequent sulfation of unsaturated fatty acids or long-chain alkanes (Tao et al., 2014; Riva et al., 2016b; Shang et al., 2016).

3.1.2 CHONS species

Although CHONS species contributed less to the total OrgS intensity than CHOS species, their nitrogen-containing molecular structures suggest their potential importance in the atmospheric nitrogen cycle, acting as important reservoirs for organic nitrogen. As shown in Table S3, a total of 895, 787, and 1277 CHONS molecular formulas were assigned in suburban summer, urban summer, and urban winter aerosol samples, respectively, accounting for 35 %, 23 % and 26 % of the total intensity of OrgSs, respectively, which underscores that CHONS species were an important component of particulate OrgSs in suburban atmospheric environments. In winter, the average MW_w, O/C_w, and DBE_w values of CHONS compounds were 322 ± 9.08, 0.65 ± 0.17, and 6.02 ± 2.60, respectively (Table S3), which were higher than those of CHOS compounds (MW_w: 285 ± 15.4, O/C_w: 0.45 ± 0.06, DBE_w: 2.56 ± 0.47). The higher MW_w and O/C_w values are probably due to the presence of additional nitrooxy (-ONO_2) functional groups, whereas the elevated DBE_w values may arise from both the formula-derived contribution of nitrooxy groups and a greater degree of carbon skeleton unsaturation (Wang et al., 2019; Lin et al., 2012b). This trend was also observed in suburban and urban summer samples. Similar to CHOS species, the DBE_w values of CHONS species in urban winter were 1.23 and 1.41 times higher than those observed in urban and suburban summer, respectively, while their average O/C_w values were lower in urban winter. Moreover, CHONS species in suburban summer were characterized by the highest H/C_w and O/C_w ratios, and the lowest DBE_w and X_{cw} values. These results indicate that the molecular distributions of CHONS species were likely shaped by seasonal and spatial differences in emission sources and atmospheric oxidative capacity. Additionally, the results from the comparison between the average H/C_w and O/C_w ratios of CHONS compounds and those reported previously were consistent with those observed for CHOS species (Table S5). For example, the O/C_w ratios of CHONS compounds here were lower than those reported in six Chinese megacities (Wang et al., 2024a).

CHONS species were primarily dominated by those with more than 6 oxygen atoms (45 %–75 % in total) on individual days (Fig. S8a). In summer, the number of CHONS species containing O ≥ 10 was substantially higher than in winter, likely attributable to enhanced photochemical oxidation processes during the summer (Cai et al., 2020; Fan et al., 2022). Furthermore, the suburban site exhibited a notably higher number of CHONS species with O ≥ 10 compared to the urban site during the summer. This spatial discrepancy may be associated with reduced NO titration effects, higher O_3 exposure (Table S1), and more abundant biogenic precursor emissions in the suburban atmosphere (Surratt et al., 2008; Wang et al., 2020b). The identified CHONS compounds spanned $N_1S_1O_1$–$N_1S_1O_{12}$ and $N_2S_1O_1$–$N_2S_1O_{12}$, with $N_1S_1O_7$ class exhibiting the highest relative abundance. Their DBE and carbon number distributions closely resembled those of CHOS species (Fig. 2a–c). Although CHONS compounds containing two N atoms were also identified, their relatively low intensity suggests a minor contribution compared to those with one N atom. The average DBE_w of $CHON_2S_1$ species was approximately 3–4 times higher than that of $CHON_1S_1$ compounds at both sites, implying that $CHON_2S_1$ probably contains numerous aromatic NOSs, whereas $CHON_1S_1$ species are predominantly composed of NOSs featuring long aliphatic carbon chains with low degrees of oxidation and unsaturation (Fig. 2a–c and Table S3). Based on the (DBE–N) value, which serves as a more reliable indicator of aromaticity (Lin et al., 2012b), CHONS compounds were dominated by olefinic species (DBE–N = 2 / 3), followed by saturated aliphatic (DBE–N ≤ 1) and aromatic (DBE–N ≥ 4) compounds. Notably, the most abundant saturated aliphatic and olefinic CHONS species fell within the C_8–C_{12} range with O ≥ 7 (Fig. 2e). $C_{10}H_{17}NO_7S$ ($m/z = 294.0653$, DBE = 3; Figs. 2c and S9) was the most abundant CHONS formulas across most samples. This species has been reported as a product of α-pinene oxidation in chamber studies (Surratt et al., 2008). Nevertheless, recent evidence has confirmed its presence in coal combustion-generated aerosols (Song et al., 2018a), suggesting this compound likely has mixed sources in polluted environments. The tentatively assigned NOSs contributed comparably to the total number of CHONS species across both sites, accounting for 56 %–60 %, which was notably lower than that of OSs in CHOS species (83 %–88 %) (Table S3). The intensity fraction of NOSs in CHONS species

was higher at the urban site (89 % ± 10 %) than at the suburban site (73 % ± 10 %) during summer. This disparity can plausibly be attributed to elevated NO_x levels in the urban environment (Table S1), which promote NOS formation via reactions with CHOS species or other organic precursors in the presence of acidic aerosols (Hamilton et al., 2021; Fan et al., 2022; Surratt et al., 2008). This result also revealed that other N- or S-containing heteroatom compounds in CHONS species, such as those derived from the oxidation of pyrrole and thiophene (Jiang et al., 2019), contributed a smaller intensity fraction at the urban site (11 % ± 2 %) than at the suburban site (27 % ± 4 %).

3.2 Potential precursor assignment of organosulfur species

The detected OSs were classified into four groups based on their potential precursors, including BVOC-derived OSs (e.g., isoprene/monoterpene/sesquiterpene-derived OSs and other BVOC-derived OSs from the precursors of green leaf volatiles), anthropogenic VOCs (AVOC)-derived OSs from the precursors of PAHs and anthropogenically emitted alkanes, multiple-sources-derived OSs, and OSs with unidentified precursors. The potential precursors of multiple-sources-derived OSs include carbonyl compounds (e.g., glyoxal and glycolaldehyde), unsaturated fatty acids, and long-chain alkenes emitted from biogenic and/or anthropogenic sources (Passananti et al., 2016; Shang et al., 2016; Fu et al., 2008). The precursor assignment of OSs was performed by matching the measured OS molecular formulas to the published OSs whose precursors have been verified. This approach has been widely used because its feasibility relies on the high mass resolution of HR-MS, which enables reliable mass peak detection and the assignment of formulas within a narrow mass tolerance (Cai et al., 2020; Wang et al., 2019; Yang et al., 2023). Details of these OS formulas with the determined precursors are listed in Tables S6–S10.

Figure 3e shows the intensity distribution of OSs derived from various precursors among the three campaigns. A total of 270 OS molecular formulas could be assigned to potential precursors, accounting for approximately 70 % of the total CHOS intensity. Among them, BVOC-derived OSs contributed 32 % ± 13 % in suburban summer, 30 % ± 12 % in urban summer, and 28 % ± 6.7 % in urban winter, whereas AVOC-derived OSs accounted for 16 % ± 4.6 %, 18 % ± 4.7 %, and 20 % ± 2.4 %, respectively. These results are consistent with the molecular signatures discussed above, suggesting relatively stronger biogenic contributions in suburban and urban summer, but enhanced anthropogenic influences in urban winter. Monoterpene-derived OSs constituted the dominant fraction of BVOC-derived OSs. Several highly abundant formulas of monoterpene-derived OSs, including $C_9H_{16}O_6S$ (m/z 251.0595), $C_{10}H_{18}O_5S$ (m/z 249.0802), and $C_9H_{16}O_7S$ (m/z 267.0544), and $C_{10}H_{18}O_7S$ (m/z 281.0701), have been frequently reported in ambient aerosols and are commonly attributed to acid-catalyzed reactions of monoterpene oxidation products (Wang et al., 2020b; Brüggemann et al., 2020b; Surratt et al., 2008). By contrast, isoprene-derived OSs contributed a much smaller fraction to the total CHOS intensity than monoterpene-derived OSs.

For identified AVOC-derived OSs, aromatic-derived OSs contributed only minor fractions to the total CHOS intensity in suburban summer (1.3 % ± 0.4 %), urban summer (1.5 % ± 0.6 %), and urban winter samples (1.9 % ± 0.7 %), whereas long-chain alkane-derived OSs accounted for much larger fractions (15 % ± 4.5 %, 17 % ± 4.6 %, and 18 % ± 2.4 %, respectively). Polycyclic aromatic hydrocarbons have been recognized as important precursors of aromatic OSs based on laboratory and field evidence (Riva et al., 2015; Kundu et al., 2013). Aromatic OSs with benzyl and polycyclic aromatic carbon backbones, such as $C_6H_6O_4S$, $C_7H_6O_4S$, $C_7H_8O_4S$, $C_8H_8O_4S$, and $C_9H_{12}O_5S$ derived from the photooxidation of naphthalene and 2-methylnaphthalene (Riva et al., 2015), have been widely observed in urban and semi-rural fine aerosols worldwide (Jiang et al., 2022; Yang et al., 2023; Wang et al., 2019; Brüggemann et al., 2020b), and were also detected in our samples. Nevertheless, despite their frequent occurrence, only a few aromatic OSs with relatively low intensity could currently be unambiguously classified. In contrast, aromatic CHOS species with $X_c \geq 2.5$ accounted for 16 % ± 3.8 % and 19 % ± 2.9 % of total CHOS species by number in suburban and urban summer, respectively, and increased to 22 % ± 3.4 % in urban winter, suggesting enhanced anthropogenic emissions in winter. The intensity fractions of aromatic CHOS in Shanghai (7 %–18 %) were comparable to those reported for Guangzhou (9 %–20 %) (Jiang et al., 2022), further underscoring a non-negligible influence of anthropogenic emissions on the molecular composition of atmospheric OrgSs in Chinese megacities. In addition, multiple-source OSs contributed similarly to total CHOS intensity in suburban summer (22 % ± 7.2 %) and urban summer (23 % ± 6.8 %), but exhibited a moderately higher contribution in urban winter (27 % ± 6.9 %). This may suggest a greater influence of anthropogenic emissions on their sources and formation processes in winter.

The precursors for 28 % ± 15 % of OS molecular formulas cannot yet be confidently recognized. Among these, subgroup B, defined as organosulfates with $C > 8$, $DBE < 3$, and $3 < O < 7$ for CHOS, contributed 6.7 % ± 3.3 %, 16 % ± 8.3 %, and 8.7 % ± 2.5 % to the total CHOS intensity in suburban summer, urban summer, and urban winter, respectively. Subgroup B is characterized by a high molecular weight, long alkyl chains, and a low degree of unsaturation and oxidation. Tao et al. (2014) speculated that the precursors of subgroup B could be long-chain alkanes from traffic emissions. Long-chain alkanes can undergo rapid photooxidation under typical urban conditions (Yee et al., 2013; Lim and Ziemann, 2009), yielding hydroxy-

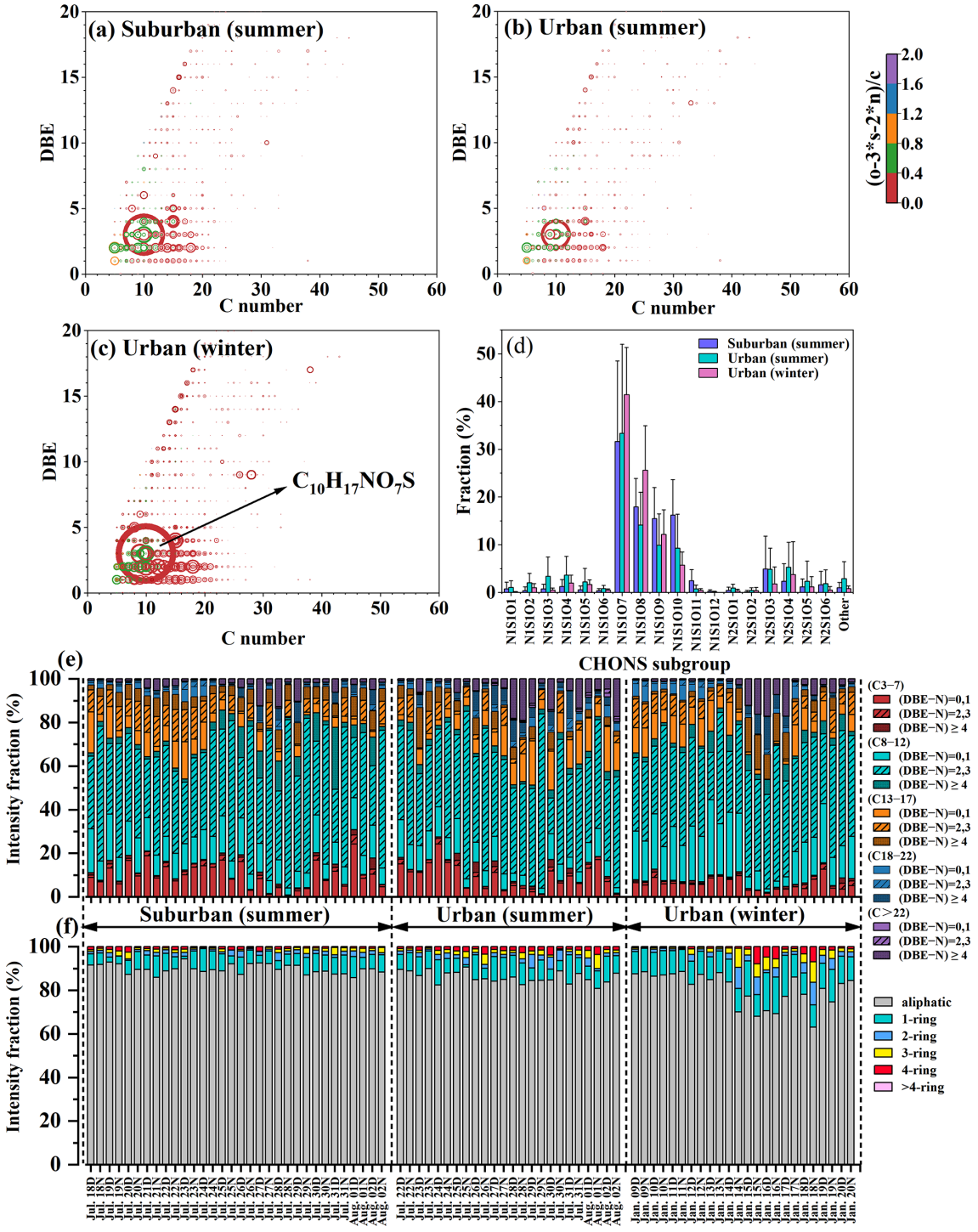

Figure 2. Molecular distribution of CHONS compounds detected by Orbitrap MS for the $PM_{2.5}$ samples collected in the three field campaigns. **(a–c)** Double-bond equivalent (DBE) vs. C number for all the CHONS compounds in the suburban (summer) and urban (summer, winter). The circle area is proportional to the square root of the relative abundance of individual molecules, and the color bar denotes the degree of oxidation. Several of the most abundant CHONS species listed in descending order by their average intensities in **(a)** are $C_9H_{15}NO_8S$, $C_{10}H_{17}NO_7S$, $C_{10}H_{17}NO_8S$, $C_{10}H_{17}NO_9S$, $C_{10}H_{17}NO_{10}S$, and $C_{15}H_{25}NO_7S$ (Fig. S9). **(d)** Classification of CHONS species into different subgroups according to the numbers of S and O atoms in their molecules. **(e)** Percentages of the intensity of each subgroup divided based on the (DBE-N) value and the length of carbon skeleton in the formulas. **(f)** Intensity percentages of each subgroup which were divided based on the X_c value of formulas.

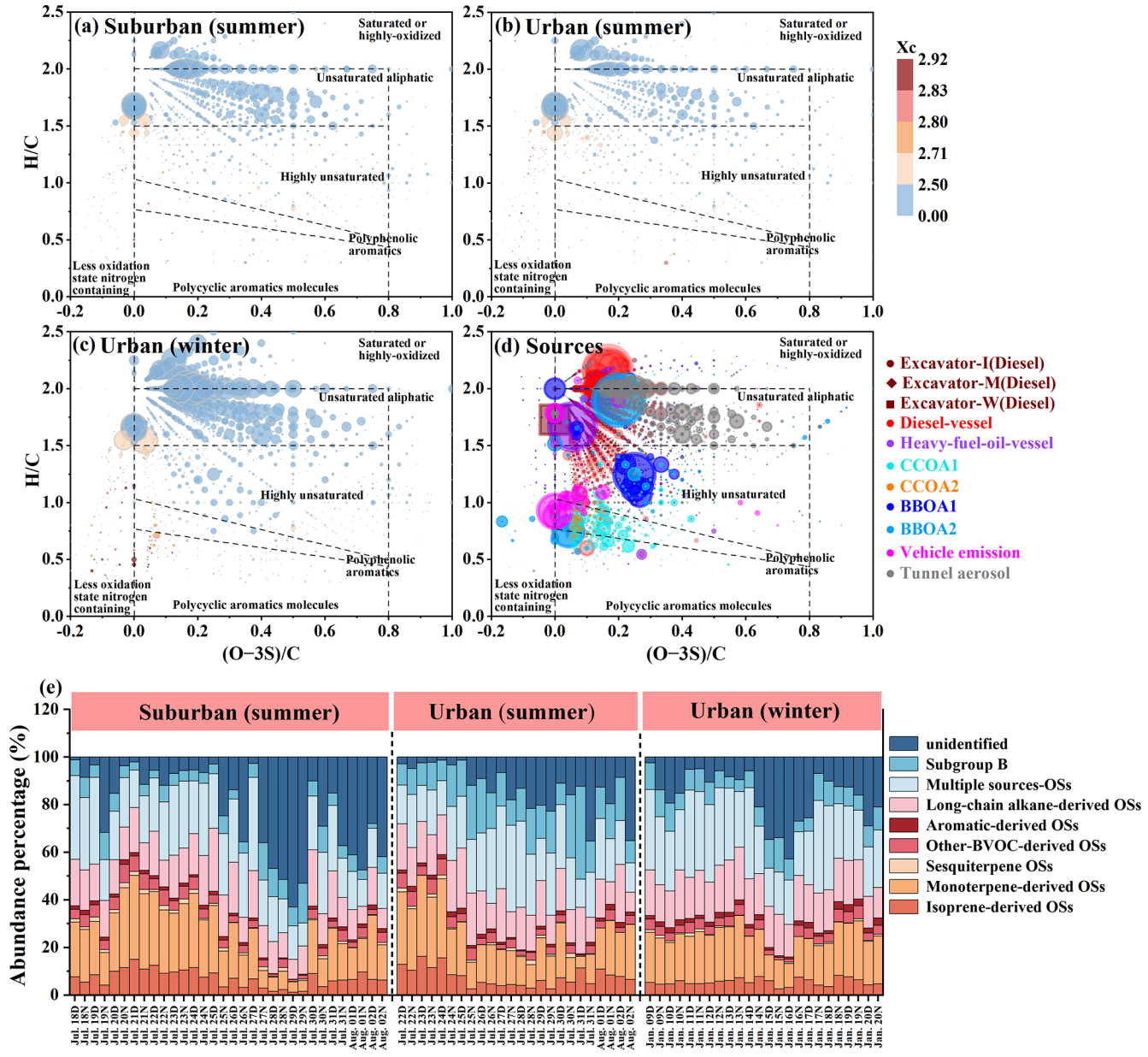

Figure 3. **(a–d)** Van Krevelen diagrams of CHOS for the field samples collected in Shanghai **(a–c)** and source samples **(d)** obtained from Cui et al. (2019) and Tang et al. (2020), including biomass burning organic aerosols (BBOAs), coal combustion organic aerosols (CCOAs), vehicle emissions, tunnel aerosols, and off-road engine emissions (excavator and vessel). Excavator-I, -M, and -W denote the operation modes of idling, moving, and working respectively. The circle area is proportional to the square root of the relative abundance of individual molecules in **(a–c)**. The marker size denotes the percentages of MS intensity to the total identified CHOS compounds in **(d)**. **(e)** Spatial, seasonal, and diurnal variations of potential precursors of detected OSs to the total intensity of identified CHOS species; subgroup B denotes OSs with unidentified precursors that satisfy $C > 8$, $DBE < 3$ and $3 < O < 7$, whereas "unidentified" denotes NOSs with unidentified precursors that fall outside these criteria.

lated or carbonylated intermediates that were further esterified to form alkyl OSs in acidic aerosol. Riva et al. (2016b), through smog-chamber photooxidation experiments of long-chain alkanes, revealed that alkane-derived OSs can also form via gaseous epoxide precursors with subsequent acid-catalyzed reactive uptake onto sulfate aerosols and/or heterogeneous reactions of hydroperoxides (Fig. 6d). Moreover, the formation of OSs from heterogeneous reactions of gaseous SO_2 with unsaturated fatty acids (USFA) was also important for these highly saturated OSs (Zhu et al., 2019; Shang et al., 2016). Large amounts of USFA have been observed in high-temperature cooking emissions, especially Chinese-style cooking with more frying, which is among the important emission sources in urban areas (Zhu et al., 2019; Zhao et al., 2015). Accordingly, subgroup B contributed more to total CHOS at the urban site ($16\,\% \pm 8.3\,\%$) than at the suburban site ($6.7\,\% \pm 3.3\,\%$) during the summer, indicating a greater influence of urban hydrocarbon emissions. Moreover, the intensity fraction of subgroup B showed positive correlations with RH (Fig. S10a), suggesting that humidity-driven heterogeneous or multiphase processing may facilitate the formation of these long-chain OSs. Although aromatic VOCs have been widely studied as drivers of particulate air pollution in densely populated regions like Shanghai (Han et al., 2023a; Gao et al., 2019), our results suggest that long-chain hydrocarbons and their corresponding OS products also play an important role in the formation of particulate organosulfurs in urban atmospheres.

In contrast to the relatively well-established precursor assignments for CHOS compounds, only a limited number of CHONS species could be linked to specific precursors (Tables S6–S10). Therefore, we further evaluated the potential precursor origins of CHONS species based on their Van Krevelen distributions, the precursor-based classification of NOSs, and molecular fingerprints from representative source samples. As shown in Fig. 4a–c, CHONS compounds, particularly NOSs, were predominantly distributed in the unsaturated aliphatic region ($H/C \approx 1.5$–2.0, $(O-3S-2N)/C \approx 0.1$–0.6), suggesting that their precursors are mainly derived from the oxidation products of BVOCs, such as isoprene and monoterpenes (Surratt et al., 2008; Lin et al., 2012b; Hamilton et al., 2021), with additional contributions from traffic-related alkenes and long-chain hydrocarbon oxidation intermediates (Tao et al., 2014; Riva et al., 2016b). The distributions of suburban and urban samples in summer were broadly similar, indicating comparable dominant precursors and formation mechanisms. In contrast, urban winter samples exhibited a more constrained distribution toward lower $(O-3S-2N)/C$ values, indicating a less oxygenated CHONS composition. This seasonal feature may partly reflect a greater contribution from NO_3-initiated oxidation under wintertime conditions characterized by elevated NO_x, lower temperatures, and weaker photochemical activity (Brown and Stutz, 2012; Hamilton et al., 2021). Figure 5e shows that seasonal variability was more influential than spatial differences in shaping NOS composition. Monoterpene-derived NOSs predominated in most samples (11 %–78 %), underscoring monoterpenes as important precursors of NOSs, which aligns with previous studies (Surratt et al., 2008; Lin et al., 2012b). In contrast, the relative contribution of isoprene-derived NOSs decreased markedly in urban winter, likely due to reduced isoprene emissions under low-temperature conditions (Guenther et al., 2012; Li et al., 2011). Furthermore, monoterpene-derived NOSs exhibited noticeable day-night variability, especially in summer, with generally higher contributions at night (Figs. 4e and S9), which is consistent with an important role of nighttime NO_3-initiated oxidation in NOS formation (Ng et al., 2017; Brown and Stutz, 2012).

To further constrain the possible precursor origins of CHONS, we compared their molecular characteristics with those reported for representative source samples in previous studies, including coal combustion organic aerosols (CCOAs), biomass burning organic aerosols (BBOAs), vehicle emissions, tunnel aerosols, and emissions from nonroad excavators and ships (Cui et al., 2019; Tang et al., 2020). As shown in Fig. 4a–d, substantial overlap in CHONS species was observed between our field samples and previously reported source samples, particularly in the high H / C region. However, ambient samples extended toward more oxidized regions, indicating that CHONS species are predominantly formed via secondary processes rather than direct primary emissions. The most abundant CHONS species in Shanghai were dominated by unsaturated aliphatic compounds (Fig. 4a–d), whose overall characteristics more closely resembled those of tunnel aerosol samples that had likely undergone atmospheric aging processes. By contrast, CHONS compounds in fresh vehicle emissions were abundant in aromatics, with 59 % of the identified CHONS species showing $X_c \geq 2.50$ (Table S12). Likewise, a large number of aromatic and highly unsaturated CHONS species were detected in both BBOAs and CCOAs, but their molecular characteristics differed substantially from the dominant CHONS components observed in Shanghai. Notably, although approximately 36 %, 40 %, and 44 % of CHONS species by number could be classified as aromatic organosulfur compounds in suburban summer, urban summer, and urban winter, respectively, most of these species exhibited relatively low abundances (Fig. 4a–d and Table S12). Thus, although combustion sources can directly emit a large variety of CHONS compounds, the low-oxidation and aromatic CHONS species that dominate the source samples contributed only weakly to the MS intensity of the ambient CHONS pool observed here. These results suggest that the CHONS in Shanghai may be less influenced by primary emissions and more likely driven by secondary formation processes, such as secondary formation via combustion-emitted precursors. Similar features were also observed in the comparison between CHOS species detected in our field samples and source samples (Fig. 3 and Table S11).

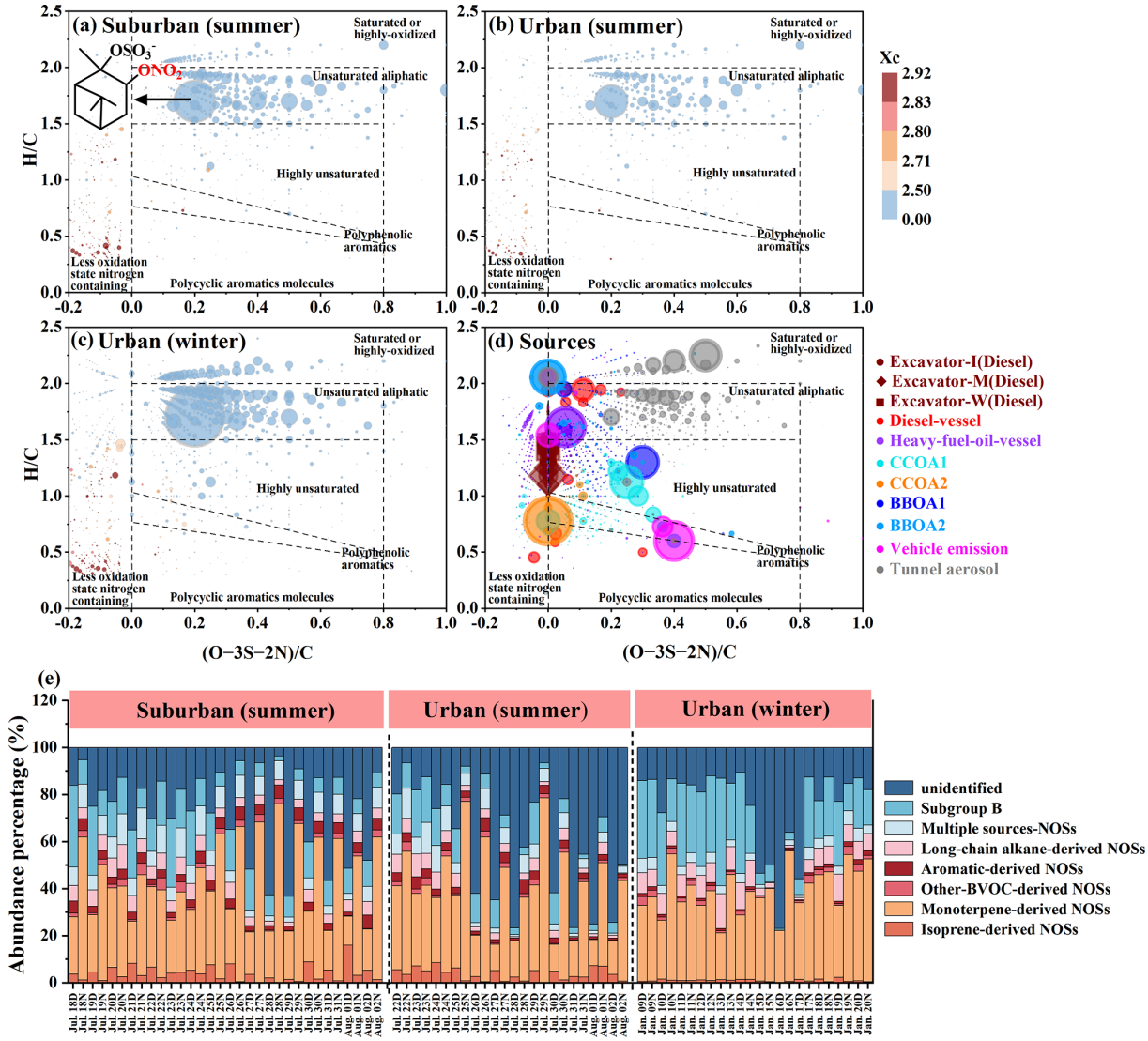

Figure 4. **(a–d)** Van Krevelen diagrams of CHONS for the field samples collected in Shanghai **(a–c)** and source samples **(d)** obtained from Cui et al. (2019) and Tang et al. (2020), including biomass burning organic aerosols (BBOAs), coal combustion organic aerosols (CCOAs), vehicle emissions, tunnel aerosols, and off-road engine emissions (excavator and vessel). Excavator-I, -M, and -W denote the operation modes of idling, moving, and working respectively. The circle area is proportional to the square root of the relative abundance of individual molecules in **(a)**–**(c)**. The marker size denotes the percentages of MS intensity to the total identified CHONS compounds in **(d)**. **(e)** Spatial, seasonal, and diurnal variations of potential precursors of detected NOSs to the total intensity of identified CHONS species; subgroup B denotes NOSs with unidentified precursors that satisfy $C > 8$, $DBE < 3$ and $6 < O < 10$, whereas "unidentified" denotes NOSs with unidentified precursors that fall outside these criteria.

Taken together, the precursor assignment and source comparison highlight the important role of secondary formation from both biogenic and anthropogenic precursors in shaping the molecular composition of particulate OrgSs in Shanghai. Given that isoprene- and monoterpene-derived OSs and NOSs are representative BVOC-derived species and are sensitive to variations in precursor emissions, oxidant regimes, NO_x / NO_3 chemistry, and sulfate-related multiphase processing, their spatial, seasonal, and day-night variability was further examined.

3.3 Spatiotemporal variability of isoprene/monoterpene-derived OSs and NOSs

During summer, isoprene/monoterpene-derived OSs at both suburban and urban sites exhibited distinct day-night variations, with significantly higher relative abundance during the day than at night ($p < 0.05$; Fig. 5a, b). This daytime enhancement is consistent with stronger photochemical processing of biogenic precursors under higher temperatures and more intense solar radiation, potentially in-

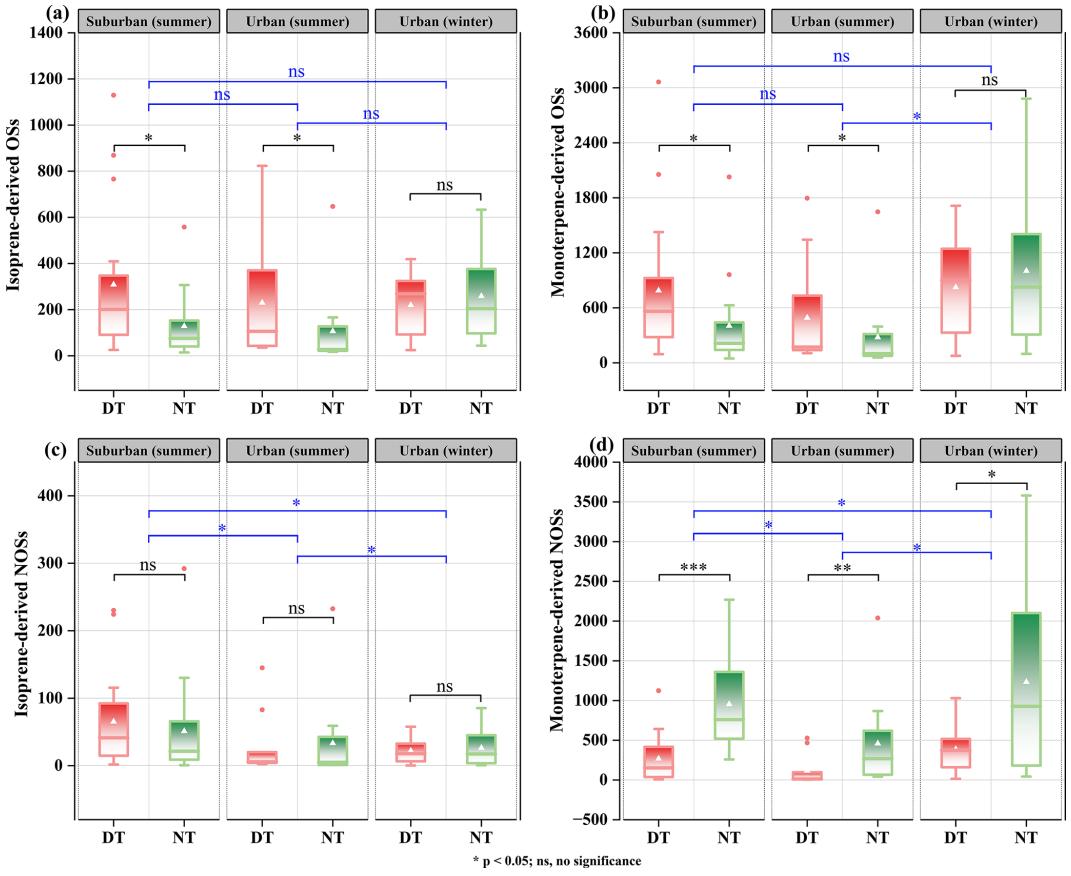

Figure 5. Spatial, seasonal, and day-night variability of isoprene- and monoterpene-derived OSs **(a, b)** and NOSs **(c, d)**. The y-axis represents the relative abundances of monoterpene/isoprene-derived OSs and NOSs, defined as peak areas normalized to the internal standard. The whisker plot boundaries are between the 10th and 90th percentiles, the box displays the 25th, 50th (median), and 75th percentiles, and the triangles display the mean values. Asterisks denote statistical significance ($^{*}p < 0.05$, $^{**}p < 0.01$, $^{***}p < 0.001$), while "ns" indicates no significance.

volving •OH-initiated oxidation (Surratt et al., 2010; Xu et al., 2015). In contrast, no significant day-night variation was observed in winter urban samples ($p > 0.05$), suggesting that the formation of these OS species in winter was less controlled by a single photochemical pathway and more influenced by multiple pathways under low-temperature, weak-radiation, and high-NO_x conditions. Notably, isoprene-derived OSs showed only weak seasonal differences, whereas monoterpene-derived OSs were more abundant in winter than in summer (Fig. 5a, b). This appears to suggest that enhanced nighttime and/or heterogeneous production in winter may partially compensate for the decline in photochemical efficiency. Recent studies have suggested that OSs could also be formed through heterogeneous or multiphase reactions between SO_2 and monoterpene-derived SOA or unsaturated fatty acids in the particle phase (Fig. 6b) (Yao et al., 2019; Zhu et al., 2019). The level of SO_2 during the winter campaign was 1.6–1.8 times higher than those during the summer campaigns (Table S1), suggesting the possible involvement of SO_2-related heterogeneous chemistry in the wintertime enhancement of monoterpene-derived OSs, although this pathway cannot be confirmed from SO_2 concentrations alone. We cannot exclude the possibility that aqueous-phase processing, aerosol acidity, and temperature-dependent gas-particle partitioning also contributed to the observed seasonal variation. These SO_2-involved heterogeneous pathways may warrant consideration under high-organic peroxide and high-SO_2 conditions (Yao et al., 2019) as well as under weakly acidic or low-RH conditions, when acid-catalyzed aqueous-phase OS formation could be limited by weak aerosol acidity or slow particle-phase reaction kinetics (Liu et al., 2017; Shiraiwa et al., 2011). Further field observations of these OSs and intermediates indicative of pathways are needed to assess the plausibility and relative importance of the proposed pathways under different atmospheric conditions. In addition, anthropogenic combustion sources (e.g., biomass burning) may provide additional inputs of isoprene and monoterpenes, which could help sustain OS formation under cold conditions (Akagi et al., 2011; Gilman et al., 2015; Yang et al., 2025).

Overall, these results suggest that photochemistry was the dominant driver of isoprene/monoterpene-derived OS formation in summer, whereas wintertime formation was governed by a more complex, multi-pathway regime involving nocturnal NO_3• chemistry and heterogeneous or multiphase processes.

The day-night patterns of monoterpene/isoprene-derived NOSs differed markedly from those of OSs. The day–night variations of isoprene-derived NOSs were not obvious across the three field campaigns (Fig. 5c), suggesting that their formation may be jointly influenced by daytime •OH oxidation and nighttime NO_3• oxidation. In contrast, monoterpene-derived NOSs exhibited obvious nighttime enhancements ($p < 0.05$; Fig. 5d), with significantly higher relative abundances at night than during the day in both suburban and urban summer samples ($p < 0.01$). This trend underscores that •NO_3-initiated nighttime oxidation is likely an important pathway for their formation (Fig. 6e), consistent with previous field and laboratory studies highlighting the important role of NO_3• oxidation of monoterpenes in NOS formation (Hamilton et al., 2021; Surratt et al., 2008; Yang et al., 2023). Elevated nighttime NO_x levels likely further favored monoterpene-NOS formation via nighttime NO_3• oxidation (Table S1). Moreover, the lower daytime relative abundance of monoterpene-derived NOSs could be exacerbated by daytime photolysis and decomposition processes (He et al., 2011; Wang et al., 2023). Spatial and seasonal variations of monoterpene-derived NOSs further highlight these possible drivers (Figs. 5d and S9). In summer, monoterpene-derived NOSs were more abundant in suburban than in urban samples, likely reflecting a stronger biogenic influence and the greater importance of monoterpene precursors at the suburban site in the YRD (Ma et al., 2022; Wang et al., 2020a). Notably, their overall relative abundance in urban samples was higher in winter than that in summer, suggesting that a more favorable oxidation environment under high-NO_x conditions may promote the production efficiency of monoterpene-derived NOSs, partly compensating for the typically lower biogenic monoterpene emissions in winter (Wang et al., 2020b). Additionally, previous studies have shown that monoterpenes can also be emitted from biomass burning, besides their well-known biogenic emission (Akagi et al., 2011; Gilman et al., 2015), which may further contribute to the accumulation of monoterpene-derived NOSs during the cold season.

3.4 Possible formation Pathways of OrgSs and the influencing factors

Atmospheric OrgSs in Shanghai originate from diverse sources, with secondary formation serving as the dominant contributor. Despite the identification of multiple reaction pathways for OS formation, their formation mechanisms in the real atmosphere remain incompletely understood. Among the known pathways, the acid-catalyzed ring-opening reaction of epoxides derived from the oxidation of VOCs is widely recognized as a kinetically feasible and key mechanism for the atmospheric formation of OSs (Fig. 6a) (Brüggemann et al., 2020b; Cai et al., 2020). For instance, previous studies have demonstrated that high concentrations of isoprene-derived OSs observed in Beijing and Guangzhou were mainly produced through the acid-catalyzed ring-opening of isoprene epoxydiol intermediates (Wang et al., 2018b; Jiang et al., 2022). Furthermore, NOSs can be formed via the nighttime NO_3-initiated oxidation of monoterpenes on acidic sulfate seed particles (Surratt et al., 2008; Ng et al., 2017). The formation and molecular distribution of OS and NOS products may be influenced by multiple environmental factors, including precursor abundance (e.g., organic precursors and anthropogenic pollutants such as NO_x and SO_2), aerosol acidity, RH, and oxidant levels. To disentangle how these complex variables impact the molecular distribution of OrgSs across different spatiotemporal settings (suburban summer, urban summer, and urban winter), NMDS analysis of OrgSs was conducted (Fig. 7). Overall, samples from different seasons and urban/suburban sites exhibit distinct separation in the two-dimensional ordination space, indicating that the molecular composition of OrgSs is highly sensitive to changes in precursor sources, oxidation conditions, and the particulate-phase reaction environment.

For suburban summer samples, Cl^- was positively correlated with the NMDS1 dimension, whereas tracers indicating combustion emissions (e.g., EC and CO), biomass burning (e.g., K^+), and secondary inorganic nitrogen species (e.g., NO_3^-), were mainly distributed on the negative direction of NMDS1 (Fig. 7a). This suggests that the NMDS1 dimension may reflect the integrated influence of different air mass sources on the molecular composition of OrgSs. It should be noted that Cl^- can originate from both combustion sources (e.g., coal smoldering) and marine aerosols (Wu et al., 2024). Cl^- was positively correlated with Na^+, a commonly used marine tracer ($R^2 = 0.69$, $p < 0.01$; Fig. S11), suggesting a potential contribution from marine air masses or sea-salt input. Nevertheless, the observed Cl^- / Na^+ mass ratios were far below the seawater value of approximately 1.80 (Keene et al., 1986; May et al., 2016), indicating that particulate Cl^- was likely affected by chloride depletion during atmospheric aging (Yao et al., 2003; Hsu et al., 2007). Given that the sampling site was situated in a coastal region and that Cl^- exhibits an opposite trend to typical combustion tracers like EC, Cl^- is more likely to represent the influence of marine air masses or sea-salt input. Therefore, the divergent trends of Cl^- and EC along the NMDS1 axis may highlight the distinct impacts of anthropogenic versus marine sources on the molecular composition of OrgSs in suburban summer. Notably, the suburban summer samples exhibited a pronounced day-night separation along the NMDS2 dimension. Daytime samples primarily clustered along the positive axis of NMDS2 and were associated with T and O_3, whereas nighttime samples aggregated in the negative direction and

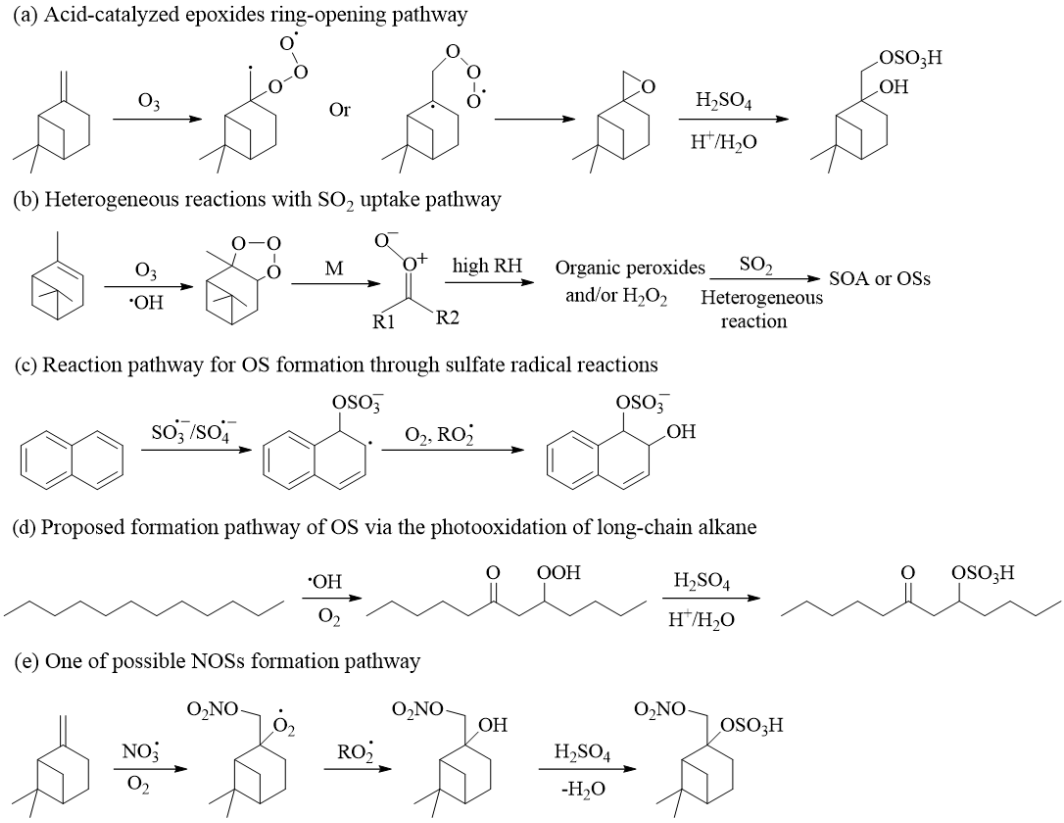

Figure 6. Potential formation mechanisms of OSs and NOSs in Shanghai (Ye et al., 2018; Brüggemann et al., 2020b; Surratt et al., 2008; Brüggemann et al., 2020a). **(a)** Proposed OSs formation pathway for acid-catalyzed ring-opening of epoxides. **(b)** Proposed OSs formation pathway for ozonolysis of unsaturated hydrocarbon in the presence of SO_2 at high relative humidity. **(c)** Reaction pathway for OSs formation through sulfate radical reactions. **(d)** One of the possible OSs formation pathways by long-chain alkanes (Riva et al., 2016b). **(e)** One of the possible NOSs formation pathways.

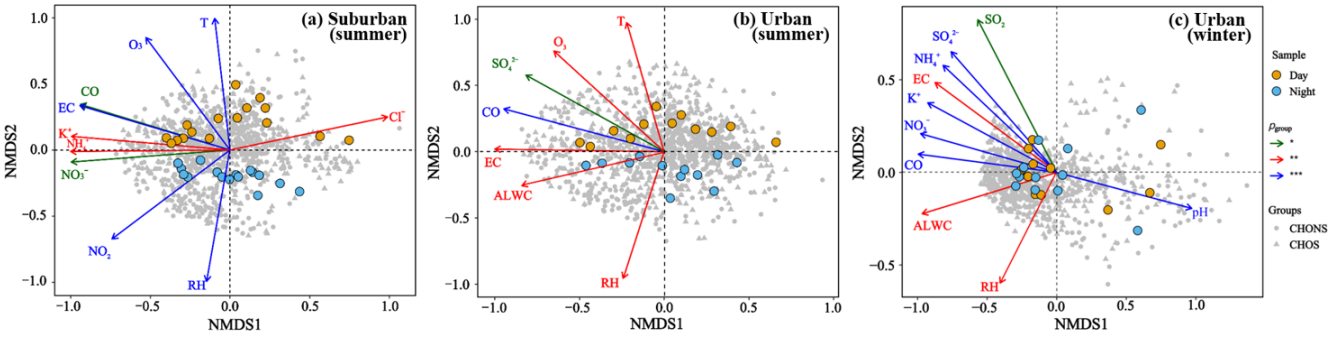

Figure 7. Nonmetric multidimensional scaling (NMDS) analysis of environmental drivers for the molecular distributions of organosulfur compounds in suburban summer **(a)**, urban summer **(b)**, and urban winter **(c)**. The two-dimensional ordinations are based on Bray–Curtis dissimilarity (stress < 0.15, nonlinear $r^2 = 0.99$) using sum-normalized intensities of individual compounds. Gray triangles and circles represent CHOS and CHONS compounds, respectively. Only significant environmental variables are shown, with color-coded vectors indicating levels of significance: $p < 0.05$ (green), $p < 0.01$ (red), and $p < 0.001$ (blue).

were associated with RH and NO_2. These associations are consistent with a greater influence of high temperature and photochemical oxidation processes on the molecular composition of OrgSs during the daytime. In summer, elevated daytime temperatures facilitate the emission of VOCs, especially BVOCs, while enhanced photochemical activity and O_3 levels may promote the oxidation of VOCs and the subsequent formation of OSs. In contrast, RH and NO_2 appeared to be the environmental factors most strongly associated with nighttime OrgS composition. On one hand, RH may affect OS formation by influencing the uptake of gaseous precursors like SO_2 by VOCs (Ye et al., 2018; Li et al., 2024a; Nestorowicz et al., 2018). On the other hand, NO_2 and its associated nighttime oxidative system (e.g., NO_3 radical) may jointly influence the formation of both OSs and NOSs by modifying the oxidation pathways and product branching of organic precursors, as well as through competition or coupling with heterogeneous processes involving sulfate and acidic particles (Hamilton et al., 2021; Fan et al., 2022).

For urban summer samples, primary combustion sources related to anthropogenic activities also appeared to play an important role in shaping the molecular composition of OrgSs, whereas the influence of marine air masses was comparatively weak. In contrast to the prominent role of inorganic nitrogen in suburban summer samples, SO_4^{2-} showed a stronger association with the molecular distribution of urban OrgSs (Fig. 7b). This observation aligns with previous studies in Shanghai and other polluted regions that have highlighted the importance of sulfate-related processes in OS formation (Yang et al., 2023; Wang et al., 2018b). SO_4^{2-} acts not only as a critical reactant but also as a regulator of particle acidity and ALWC, which in turn affects the reactive uptake and heterogeneous conversion efficiency of precursors (Wang et al., 2021b). The distinct influences of different anthropogenic emission species on OrgSs distribution between urban and suburban summer underscore the varying impact of human activities on OS formation across different environments. Nevertheless, the environmental factors associated with day-night variations in OrgS composition were generally similar between the two sites. Daytime samples clustered with T and O_3 along the positive axis of NMDS2, while nighttime samples aggregate with RH along the negative axis. This result suggests that site type had only a limited influence on the day-night distribution of OrgSs in summer. The main processes potentially governing the day-night variability of OrgSs appeared to be broadly similar across the two sites, mainly involving enhanced photochemical oxidation during the daytime and RH-dependent multiphase processing at night.

For urban winter samples, the potential factors influencing the molecular distribution of OrgSs were more complex than those in summer (Fig. 7c). In addition to the impact of primary anthropogenic emissions, inorganic nitrogen and sulfur species were significantly associated with wintertime OrgS composition, clustering along the negative axis of NMDS1. ALWC is also distributed in the negative NMDS1 direction, suggesting that it was another environmental factor associated with the wintertime molecular distribution of OrgSs. ALWC is influenced not only by RH, but also by the loading of hygroscopic inorganic components such as NO_3^- and SO_4^{2-}. Under the humid and polluted conditions typical of winter, the accumulation of these species can significantly enhance ALWC and thereby favor aqueous-phase processing (Wang et al., 2021b). Previous mechanistic and field studies suggest that elevated ALWC may promote the mass transfer and reactive uptake of SO_2 and oxidized organic intermediates into the particle phase, while also providing a medium for subsequent aqueous-phase transformations (Li et al., 2025; Yao et al., 2019; Wang et al., 2021b). Aerosol pH was also significantly associated with wintertime OrgS composition. Lower pH can favor the reactive uptake of epoxides and other oxidative intermediates onto acidic sulfate particles and may facilitate aqueous-phase esterification via acid-catalyzed mechanisms (Wang et al., 2018b). Taken together with previous mechanistic evidence, the observed associations of wintertime OrgS composition with ALWC and aerosol acidity are consistent with the potential importance of multiphase and acid-catalyzed processing in the secondary formation and molecular evolution of urban OrgSs in winter. Overall, source-related associations differed between sites, with suburban OrgSs linked to marine and combustion influences and urban OrgSs more closely associated with anthropogenic emissions and sulfate-related processes. The molecular composition of OrgSs in summer was more closely associated with photochemical oxidation during the daytime and RH-dependent heterogeneous processes at night, whereas wintertime OrgSs appeared to be more strongly influenced by the combined effects of enhanced primary emissions, the accumulation of secondary inorganic species, and the synergistic regulation of the particle-phase reaction environment by ALWC and pH.

4 Conclusions and atmospheric implications

This study provides a molecular-level characterization of atmospheric organosulfur compounds (OrgSs) in Shanghai under contrasting atmospheric environments, including suburban summer, urban summer, and urban winter. A total of 1964, 1914, and 2689 OrgS molecular formulas were detected in suburban summer, urban summer, and urban winter aerosol samples, respectively. OrgSs were dominated by $CHOS_1$ and $CHON_1S_1$ species, which together accounted for most of the detected formulas and signal intensity. As many as 79 %–92 % of OrgS species had the elemental composition of $(4s + 3n)/o \leq 1$ in their formulas, suggesting that they were potential OSs or nitrooxy-OSs. The molecular characteristics of both CHOS and CHONS exhibited pronounced seasonal variability. Compared with summer, wintertime OrgSs showed lower O / C ratios but higher DBE val-

ues and aromaticity, suggesting a larger contribution from anthropogenic emissions and more unsaturated structures under winter conditions. Although aliphatic structures dominated the OrgS pool overall, the increased abundance of aromatic and polyaromatic species in winter further pointed to enhanced combustion-related influences during the cold season.

Potential precursor analysis showed that BVOC-derived OSs were the largest identified group, followed by OSs derived from anthropogenic VOCs and mixed-source precursors. Monoterpene-derived OSs dominated the biogenic fraction, while the intensity fraction of isoprene-derived OSs increased in summer, especially at the suburban site. In contrast, aromatic and long-chain alkane-derived OSs increased in winter, highlighting a stronger anthropogenic influence. CHONS species showed weaker similarity to primary source profiles and appeared to be more strongly affected by secondary formation, although combustion emissions may still provide important precursors in polluted environments.

The diurnal and seasonal behaviors of isoprene/monoterpene-derived OSs and NOSs may reflect distinct formation pathways. Isoprene/monoterpene-derived OSs peaked during the daytime in summer, likely reflecting stronger photochemical processing, whereas monoterpene-derived NOSs were significantly enhanced at night in both summer and winter, consistent with a potential contribution from NO_3-initiated oxidation. The NMDS results further showed that the molecular composition of OrgSs was highly sensitive to seasonal, spatial, and day-night changes in precursor sources, oxidant levels, and particle-phase reaction conditions. In summer, the NMDS1 patterns indicated contrasting source-related associations: suburban OrgS composition was influenced by both marine air masses and combustion-related emissions, whereas urban OrgSs were more closely associated with anthropogenic emissions and sulfate-related processes. The NMDS2 patterns revealed broadly similar day-night variations at the two sites, with daytime OrgS composition mainly associated with temperature and O_3 and nighttime composition more closely linked to RH and NO_2. These associations are consistent with potential contributions from photochemical processing during the daytime and from RH-dependent multiphase processing and NO_3-initiated oxidation at night. The similar day-night separation observed at the suburban and urban sites implies that the dominant mechanisms controlling summer day-night variability were broadly consistent across different functional zones. In winter, the molecular distribution of OrgSs became more strongly associated with inorganic nitrogen and sulfur species, ALWC, and aerosol acidity, highlighting the potential importance of multiphase and acid-catalyzed processing under polluted winter conditions. Together, these observations suggest that the formation of atmospheric OrgSs in Shanghai is jointly regulated by precursor availability, oxidation pathways, and the physicochemical properties of the particle phase. Overall, this study provides new molecular-level evidence that improves our understanding of the sources, formation pathways, and associated environmental factors of atmospheric OrgSs, with implications for interpreting aerosol evolution and for better representing organosulfur chemistry in atmospheric models.

Data availability. Data are available upon request from the corresponding author.

Supplement. The supplement related to this article is available online at https://doi.org/10.5194/acp-26-11067-2026-supplement.

Author contributions. D. C. and X. G. conceived and designed the study. S. Z. and Y. C. carried out the field sampling. D. C., S. R., and Y. F. performed the UHPLC-Orbitrap MS analysis and data processing. X. G. and J. C. acquired funding and undertook project management. D. C. prepared the manuscript with contributions from all co-authors.

Competing interests. The contact author has declared that none of the authors has any competing interests.

Disclaimer. Publisher's note: Copernicus Publications remains neutral with regard to jurisdictional claims made in the text, published maps, institutional affiliations, or any other geographical representation in this paper. The authors bear the ultimate responsibility for providing appropriate place names. Views expressed in the text are those of the authors and do not necessarily reflect the views of the publisher.

Acknowledgements. We gratefully acknowledge the support of the Key Laboratory of Atmospheric Particle Pollution and Prevention of Fudan University.

Financial support. This research has been supported by the National Natural Science Foundation of China (grant no. 42505104, 22336001).

Review statement. This paper was edited by Ivan Kourtchev and reviewed by four anonymous referees.

References

Akagi, S. K., Yokelson, R. J., Wiedinmyer, C., Alvarado, M. J., Reid, J. S., Karl, T., Crounse, J. D., and Wennberg, P. O.: Emission factors for open and domestic biomass burning for use in atmospheric models, Atmos. Chem. Phys., 11, 4039–4072, https://doi.org/10.5194/acp-11-4039-2011, 2011.

Brown, S. S. and Stutz, J.: Nighttime radical observations and chemistry, Chem. Soc. Rev., 41, 6405–6447, https://doi.org/10.1039/c2cs35181a, 2012.

Brüggemann, M., Riva, M., Perrier, S., Poulain, L., George, C., and Herrmann, H.: Overestimation of Monoterpene Organosulfate Abundance in Aerosol Particles by Sampling in the Presence of SO_2, Environ. Sci. Tech. Let., https://doi.org/10.1021/acs.estlett.0c00814, 2020a.

Brüggemann, M., Xu, R., Tilgner, A., Kwong, K. C., Mutzel, A., Poon, H. Y., Otto, T., Schaefer, T., Poulain, L., Chan, M. N., and Herrmann, H.: Organosulfates in Ambient Aerosol: State of Knowledge and Future Research Directions on Formation, Abundance, Fate, and Importance, Environ. Sci. Technol., 54, 3767–3782, https://doi.org/10.1021/acs.est.9b06751, 2020b.

Cai, D., Wang, X., Chen, J., and Li, X.: Molecular Characterization of Organosulfates in Highly Polluted Atmosphere Using Ultra-High-Resolution Mass Spectrometry, J. Geophys. Res.-Atmos., 125, https://doi.org/10.1029/2019jd032253, 2020.

Cai, D., Li, C., Lin, J., Sun, W., Zhang, M., Wang, T., Abudumutailifu, M., Lyu, Y., Huang, X., Li, X., and Chen, J.: Comparative study of atmospheric brown carbon at Shanghai and the East China Sea: Molecular characterization and optical properties, Sci. Total Environ., 941, 173782, https://doi.org/10.1016/j.scitotenv.2024.173782, 2024.

Cui, M., Li, C., Chen, Y., Zhang, F., Li, J., Jiang, B., Mo, Y., Li, J., Yan, C., Zheng, M., Xie, Z., Zhang, G., and Zheng, J.: Molecular characterization of polar organic aerosol constituents in off-road engine emissions using Fourier transform ion cyclotron resonance mass spectrometry (FT-ICR MS): implications for source apportionment, Atmos. Chem. Phys., 19, 13945–13956, https://doi.org/10.5194/acp-19-13945-2019, 2019.

Daellenbach, K. R., Kourtchev, I., Vogel, A. L., Bruns, E. A., Jiang, J., Petäjä, T., Jaffrezo, J.-L., Aksoyoglu, S., Kalberer, M., Baltensperger, U., El Haddad, I., and Prévôt, A. S. H.: Impact of anthropogenic and biogenic sources on the seasonal variation in the molecular composition of urban organic aerosols: a field and laboratory study using ultra-high-resolution mass spectrometry, Atmos. Chem. Phys., 19, 5973–5991, https://doi.org/10.5194/acp-19-5973-2019, 2019.

Darer, A. I., Cole-Filipiak, N. C., O'Connor, A. E., and Elrod, M. J.: Formation and Stability of Atmospherically Relevant Isoprene-Derived Organosulfates and Organonitrates, Environ. Sci. Technol., 45, 1895–1902, https://doi.org/10.1021/es103797z, 2011.

Donahue, N. M., Epstein, S. A., Pandis, S. N., and Robinson, A. L.: A two-dimensional volatility basis set: 1. organic-aerosol mixing thermodynamics, Atmos. Chem. Phys., 11, 3303–3318, https://doi.org/10.5194/acp-11-3303-2011, 2011.

Fan, W., Chen, T., Zhu, Z., Zhang, H., Qiu, Y., and Yin, D.: A review of secondary organic aerosols formation focusing on organosulfates and organic nitrates, J. Hazard Mater., 430, 128406, https://doi.org/10.1016/j.jhazmat.2022.128406, 2022.

Fu, T.-M., Jacob, D. J., Wittrock, F., Burrows, J. P., Vrekoussis, M., and Henze, D. K.: Global budgets of atmospheric glyoxal and methylglyoxal, and implications for formation of secondary organic aerosols, J. Geophys. Res.-Atmos., 113, https://doi.org/10.1029/2007jd009505, 2008.

Gao, Y., Wang, H., Zhang, X., Jing, S. a., Peng, Y., Qiao, L., Zhou, M., Huang, D. D., Wang, Q., Li, X., Li, L., Feng, J., Ma, Y., and Li, Y.: Estimating Secondary Organic Aerosol Production from Toluene Photochemistry in a Megacity of China, Environ. Sci. Technol., 53, 8664–8671, https://doi.org/10.1021/acs.est.9b00651, 2019.

Gilman, J. B., Lerner, B. M., Kuster, W. C., Goldan, P. D., Warneke, C., Veres, P. R., Roberts, J. M., de Gouw, J. A., Burling, I. R., and Yokelson, R. J.: Biomass burning emissions and potential air quality impacts of volatile organic compounds and other trace gases from fuels common in the US, Atmos. Chem. Phys., 15, 13915–13938, https://doi.org/10.5194/acp-15-13915-2015, 2015.

Guenther, A. B., Jiang, X., Heald, C. L., Sakulyanontvittaya, T., Duhl, T., Emmons, L. K., and Wang, X.: The Model of Emissions of Gases and Aerosols from Nature version 2.1 (MEGAN2.1): an extended and updated framework for modeling biogenic emissions, Geosci. Model Dev., 5, 1471–1492, https://doi.org/10.5194/gmd-5-1471-2012, 2012.

Guo, H., Xu, L., Bougiatioti, A., Cerully, K. M., Capps, S. L., Hite Jr., J. R., Carlton, A. G., Lee, S.-H., Bergin, M. H., Ng, N. L., Nenes, A., and Weber, R. J.: Fine-particle water and pH in the southeastern United States, Atmos. Chem. Phys., 15, 5211–5228, https://doi.org/10.5194/acp-15-5211-2015, 2015.

Hamilton, J. F., Bryant, D. J., Edwards, P. M., Ouyang, B., Bannan, T. J., Mehra, A., Mayhew, A. W., Hopkins, J. R., Dunmore, R. E., Squires, F. A., Lee, J. D., Newland, M. J., Worrall, S. D., Bacak, A., Coe, H., Percival, C., Whalley, L. K., Heard, D. E., Slater, E. J., Jones, R. L., Cui, T., Surratt, J. D., Reeves, C. E., Mills, G. P., Grimmond, S., Sun, Y., Xu, W., Shi, Z., and Rickard, A. R.: Key Role of NO_3 Radicals in the Production of Isoprene Nitrates and Nitrooxyorganosulfates in Beijing, Environ. Sci. Technol., 55, 842–853, https://doi.org/10.1021/acs.est.0c05689, 2021.

Han, Y., Wang, T., Li, R., Fu, H., Duan, Y., Gao, S., Zhang, L., and Chen, J.: Measurement report: Volatile organic compound characteristics of the different land-use types in Shanghai: spatiotemporal variation, source apportionment and impact on secondary formations of ozone and aerosol, Atmos. Chem. Phys., 23, 2877–2900, https://doi.org/10.5194/acp-23-2877-2023, 2023a.

Han, Y., Zhang, X., Li, L., Lin, Y., Zhu, C., Zhang, N., Wang, Q., and Cao, J.: Enhanced Production of Organosulfur Species during a Severe Winter Haze Episode in the Guanzhong Basin of Northwest China, Environ. Sci. Technol., https://doi.org/10.1021/acs.est.3c02914, 2023b.

Hansen, A. M. K., Hong, J., Raatikainen, T., Kristensen, K., Ylisirniö, A., Virtanen, A., Petäjä, T., Glasius, M., and Prisle, N. L.: Hygroscopic properties and cloud condensation nuclei activation of limonene-derived organosulfates and their mixtures with ammonium sulfate, Atmos. Chem. Phys., 15, 14071–14089, https://doi.org/10.5194/acp-15-14071-2015, 2015.

Hatch, L. E., Creamean, J. M., Ault, A. P., Surratt, J. D., Chan, M. N., Seinfeld, J. H., Edgerton, E. S., Su, Y., and Prather, K. A.: Measurements of isoprene-derived organosulfates in ambient aerosols by aerosol time-of-flight mass spectrometry-part 2: tem-

poral variability and formation mechanisms, Environ. Sci. Technol., 45, 8648–8655, https://doi.org/10.1021/es2011836, 2011.

He, S., Chen, Z., and Zhang, X.: Photochemical reactions of methyl and ethyl nitrate: a dual role for alkyl nitrates in the nitrogen cycle, Environ. Chem., 8, 529–542, https://doi.org/10.1071/en10004, 2011.

He, Y., Ding, X., He, Q., Zhang, Y., Chen, D., Zhang, T., Yang, K., Wang, J., Cheng, Q., Jiang, H., Wang, Z., Liu, P., Wang, X., and Boy, M.: Long-term Trends in $PM_{2.5}$ Chemical Composition and Its Impact on Aerosol Properties: Field Observations from 2007 to 2020 in Pearl River Delta, South China, Atmos. Chem. Phys., 25, 13729–13745, https://doi.org/10.5194/acp-25-13729-2025, 2025.

Hennigan, C. J., Izumi, J., Sullivan, A. P., Weber, R. J., and Nenes, A.: A critical evaluation of proxy methods used to estimate the acidity of atmospheric particles, Atmos. Chem. Phys., 15, 2775–2790, https://doi.org/10.5194/acp-15-2775-2015, 2015.

Hettiyadura, A. P. S., Stone, E. A., Kundu, S., Baker, Z., Geddes, E., Richards, K., and Humphry, T.: Determination of atmospheric organosulfates using HILIC chromatography with MS detection, Atmos. Meas. Tech., 8, 2347–2358, https://doi.org/10.5194/amt-8-2347-2015, 2015.

Hsu, S.-C., Liu, S. C., Kao, S.-J., Jeng, W.-L., Huang, Y.-T., Tseng, C.-M., Tsai, F., Tu, J.-Y., and Yang, Y.: Water-soluble species in the marine aerosol from the northern South China Sea: High chloride depletion related to air pollution, J. Geophys. Res.-Atmos., 112, https://doi.org/10.1029/2007JD008844, 2007.

Hu, M., Krauss, M., Brack, W., and Schulze, T.: Optimization of LC-Orbitrap-HRMS acquisition and MZmine 2 data processing for nontarget screening of environmental samples using design of experiments, Anal. Bioanal. Chem., 408, 7905–7915, https://doi.org/10.1007/s00216-016-9919-8, 2016.

Huang, L., Cochran, R. E., Coddens, E. M., and Grassian, V. H.: Formation of Organosulfur Compounds through Transition Metal Ion-Catalyzed Aqueous Phase Reactions, Environ. Sci. Tech. Let., 5, 315–321, https://doi.org/10.1021/acs.estlett.8b00225, 2018.

Huang, W., Saathoff, H., Shen, X., Ramisetty, R., Leisner, T., and Mohr, C.: Seasonal characteristics of organic aerosol chemical composition and volatility in Stuttgart, Germany, Atmos. Chem. Phys., 19, 11687–11700, https://doi.org/10.5194/acp-19-11687-2019, 2019.

Jiang, H., Frie, A. L., Lavi, A., Chen, J. Y., Zhang, H., Bahreini, R., and Lin, Y.-H.: Brown Carbon Formation from Nighttime Chemistry of Unsaturated Heterocyclic Volatile Organic Compounds, Environ. Sci. Tech. Let., 6, 184–190, https://doi.org/10.1021/acs.estlett.9b00017, 2019.

Jiang, H., Li, J., Tang, J., Cui, M., Zhao, S., Mo, Y., Tian, C., Zhang, X., Jiang, B., Liao, Y., Chen, Y., and Zhang, G.: Molecular characteristics, sources, and formation pathways of organosulfur compounds in ambient aerosol in Guangzhou, South China, Atmos. Chem. Phys., 22, 6919–6935, https://doi.org/10.5194/acp-22-6919-2022, 2022.

Jiang, H., Cai, J., Feng, X., Chen, Y., Guo, H., Mo, Y., Tang, J., Chen, T., Li, J., and Zhang, G.: Organosulfur Compounds: A Non-Negligible Component Affecting the Light Absorption of Brown Carbon During North China Haze Events, J. Geophys. Res.-Atmos., 130, https://doi.org/10.1029/2024jd042043, 2025.

Keene, W. C., Pszenny, A. A. P., Galloway, J. N., and Hawley, M. E.: Sea-salt corrections and interpretation of constituent ratios in marine precipitation, J. Geophys. Res.-Atmos., 91, 6647–6658, https://doi.org/10.1029/JD091iD06p06647, 1986.

Kellerman, A. M., Dittmar, T., Kothawala, D. N., and Tranvik, L. J.: Chemodiversity of dissolved organic matter in lakes driven by climate and hydrology, Nat. Commun., 5, 3804, https://doi.org/10.1038/ncomms4804, 2014.

Kourtchev, I., Giorio, C., Manninen, A., Wilson, E., Mahon, B., Aalto, J., Kajos, M., Venables, D., Ruuskanen, T., Levula, J., Loponen, M., Connors, S., Harris, N., Zhao, D., Kiendler-Scharr, A., Mentel, T., Rudich, Y., Hallquist, M., Doussin, J.-F., Maenhaut, W., Bäck, J., Petäjä, T., Wenger, J., Kulmala, M., and Kalberer, M.: Enhanced Volatile Organic Compounds emissions and organic aerosol mass increase the oligomer content of atmospheric aerosols, Sci. Rep.-UK, 6, https://doi.org/10.1038/srep35038, 2016.

Kundu, S., Quraishi, T. A., Yu, G., Suarez, C., Keutsch, F. N., and Stone, E. A.: Evidence and quantitation of aromatic organosulfates in ambient aerosols in Lahore, Pakistan, Atmos. Chem. Phys., 13, 4865–4875, https://doi.org/10.5194/acp-13-4865-2013, 2013.

Li, L., Li, J., Zhang, X., Lin, Y., Wang, R., Cao, J., and Han, Y.: Effects of relative humidity on atmospheric organosulfur species derived from photooxidation and nocturnal chemistry in a forest environment, Environ. Pollut., 363, https://doi.org/10.1016/j.envpol.2024.125253, 2024a.

Li, W., Qi, Y., Liu, Y., Wu, G., Zhang, Y., Shi, J., Qu, W., Sheng, L., Wang, W., Zhang, D., and Zhou, Y.: Daytime and nighttime aerosol soluble iron formation in clean and slightly polluted moist air in a coastal city in eastern China, Atmos. Chem. Phys., 24, 6495–6508, https://doi.org/10.5194/acp-24-6495-2024, 2024b.

Li, W., Ito, A., Wang, G., Zhi, M., Xu, L., Yuan, Q., Zhang, J., Liu, L., Wu, F., Laskin, A., Zhang, D., Zhang, X., Zhu, T., Chen, J., Mihalopoulos, N., Bougiatioti, A., Kanakidou, M., Wang, G., Hu, H., Zhao, Y., and Shi, Z.: Aqueous-phase secondary organic aerosol formation on mineral dust, Natl. Sci. Rev., 12, 221, https://doi.org/10.1093/nsr/nwaf221, 2025.

Li, Y., Pöschl, U., and Shiraiwa, M.: Molecular corridors and parameterizations of volatility in the chemical evolution of organic aerosols, Atmos. Chem. Phys., 16, 3327–3344, https://doi.org/10.5194/acp-16-3327-2016, 2016.

Li, Z., Ratliff, E. A., and Sharkey, T. D.: Effect of Temperature on Postillumination Isoprene Emission in Oak and Poplar, Plant Physiol., 155, 1037–1046, https://doi.org/10.1104/pp.110.167551, 2011.

Lim, Y. B. and Ziemann, P. J.: Effects of Molecular Structure on Aerosol Yields from OH Radical-Initiated Reactions of Linear, Branched, and Cyclic Alkanes in the Presence of NOx, Environ. Sci. Technol., 43, 2328–2334, https://doi.org/10.1021/es803389s, 2009.

Lin, P., Rincon, A. G., Kalberer, M., and Yu, J. Z.: Elemental composition of HULIS in the Pearl River Delta Region, China: results inferred from positive and negative electrospray high resolution mass spectrometric data, Environ. Sci. Technol., 46, 7454–7462, https://doi.org/10.1021/es300285d, 2012a.

Lin, P., Yu, J. Z., Engling, G., and Kalberer, M.: Organosulfates in humic-like substance fraction isolated from aerosols at

seven locations in East Asia: a study by ultra-high-resolution mass spectrometry, Environ. Sci. Technol., 46, 13118–13127, https://doi.org/10.1021/es303570v, 2012b.

Liu, Y., Wu, Z., Wang, Y., Xiao, Y., Gu, F., Zheng, J., Tan, T., Shang, D., Wu, Y., Zeng, L., Hu, M., Bateman, A. P., and Martin, S. T.: Submicrometer Particles Are in the Liquid State during Heavy Haze Episodes in the Urban Atmosphere of Beijing, China, Environ. Sci. Tech. Let., 4, 427–432, https://doi.org/10.1021/acs.estlett.7b00352, 2017.

Liu, Z., Gao, W., Yu, Y., Hu, B., Xin, J., Sun, Y., Wang, L., Wang, G., Bi, X., Zhang, G., Xu, H., Cong, Z., He, J., Xu, J., and Wang, Y.: Characteristics of $PM_{2.5}$ mass concentrations and chemical species in urban and background areas of China: emerging results from the CARE-China network, Atmos. Chem. Phys., 18, 8849–8871, https://doi.org/10.5194/acp-18-8849-2018, 2018.

Lukács, H., Gelencsér, A., Hoffer, A., Kiss, G., Horváth, K., and Hartyáni, Z.: Quantitative assessment of organosulfates in size-segregated rural fine aerosol, Atmos. Chem. Phys., 9, 231–238, https://doi.org/10.5194/acp-9-231-2009, 2009.

Ma, X., Tan, Z., Lu, K., Yang, X., Chen, X., Wang, H., Chen, S., Fang, X., Li, S., Li, X., Liu, J., Liu, Y., Lou, S., Qiu, W., Wang, H., Zeng, L., and Zhang, Y.: OH and HO_2 radical chemistry at a suburban site during the EXPLORE-YRD campaign in 2018, Atmos. Chem. Phys., 22, 7005–7028, https://doi.org/10.5194/acp-22-7005-2022, 2022.

Ma, Y., Xu, X., Song, W., Geng, F., and Wang, L.: Seasonal and diurnal variations of particulate organosulfates in urban Shanghai, China, Atmos. Environ., 85, 152–160, https://doi.org/10.1016/j.atmosenv.2013.12.017, 2014.

May, N. W., Quinn, P. K., McNamara, S. M., and Pratt, K. A.: Multiyear study of the dependence of sea salt aerosol on wind speed and sea ice conditions in the coastal Arctic, J. Geophys. Res.-Atmos., 121, 9208–9219, https://doi.org/10.1002/2016jd025273, 2016.

Minerath, E. C. and Elrod, M. J.: Assessing the Potential for Diol and Hydroxy Sulfate Ester Formation from the Reaction of Epoxides in Tropospheric Aerosols, Environ. Sci. Technol., 43, 1386–1392, https://doi.org/10.1021/es8029076, 2009.

Minerath, E. C., Casale, M. T., and Elrod, M. J.: Kinetics feasibility study of alcohol sulfate esterification reactions in tropospheric aerosols, Environ. Sci. Technol., 42, 4410–4415, https://doi.org/10.1021/es8004333, 2008.

Murphy, B. N., Donahue, N. M., Robinson, A. L., and Pandis, S. N.: A naming convention for atmospheric organic aerosol, Atmos. Chem. Phys., 14, 5825–5839, https://doi.org/10.5194/acp-14-5825-2014, 2014.

Nestorowicz, K., Jaoui, M., Rudzinski, K. J., Lewandowski, M., Kleindienst, T. E., Spólnik, G., Danikiewicz, W., and Szmigielski, R.: Chemical composition of isoprene SOA under acidic and non-acidic conditions: effect of relative humidity, Atmos. Chem. Phys., 18, 18101–18121, https://doi.org/10.5194/acp-18-18101-2018, 2018.

Ng, N. L., Brown, S. S., Archibald, A. T., Atlas, E., Cohen, R. C., Crowley, J. N., Day, D. A., Donahue, N. M., Fry, J. L., Fuchs, H., Griffin, R. J., Guzman, M. I., Herrmann, H., Hodzic, A., Iinuma, Y., Jimenez, J. L., Kiendler-Scharr, A., Lee, B. H., Luecken, D. J., Mao, J., McLaren, R., Mutzel, A., Osthoff, H. D., Ouyang, B., Picquet-Varrault, B., Platt, U., Pye, H. O. T., Rudich, Y., Schwantes, R. H., Shiraiwa, M., Stutz, J., Thornton, J. A., Tilgner, A., Williams, B. J., and Zaveri, R. A.: Nitrate radicals and biogenic volatile organic compounds: oxidation, mechanisms, and organic aerosol, Atmos. Chem. Phys., 17, 2103–2162, https://doi.org/10.5194/acp-17-2103-2017, 2017.

Ning, C., Tang, Y., Sun, H., Wang, D., Sun, S., and Gao, Y.: Molecular characteristics and formation pathways of organosulfates in atmospheric fine particles: A case study in steel industrial city during winter heating period, J. Hazard Mater., 495, 138882, https://doi.org/10.1016/j.jhazmat.2025.138882, 2025.

Noziere, B., Ekstrom, S., Alsberg, T., and Holmstrom, S.: Radical-initiated formation of organosulfates and surfactants in atmospheric aerosols, Geophys. Res. Lett., 37, https://doi.org/10.1029/2009gl041683, 2010.

O'Brien, R. E., Laskin, A., Laskin, J., Rubitschun, C. L., Surratt, J. D., and Goldstein, A. H.: Molecular characterization of S- and N-containing organic constituents in ambient aerosols by negative ion mode high-resolution Nanospray Desorption Electrospray Ionization Mass Spectrometry: CalNex 2010 field study, J. Geophys. Res.-Atmos., 119, 12706–12720, https://doi.org/10.1002/2014jd021955, 2014.

Passananti, M., Kong, L., Shang, J., Dupart, Y., Perrier, S., Chen, J., Donaldson, D. J., and George, C.: Organosulfate Formation through the Heterogeneous Reaction of Sulfur Dioxide with Unsaturated Fatty Acids and Long-Chain Alkenes, Angew. Chem.-Int. Edit., 55, 10336–10339, https://doi.org/10.1002/anie.201605266, 2016.

Rincón, A. G., Calvo, A. I., Dietzel, M., and Kalberer, M.: Seasonal differences of urban organic aerosol composition – an ultra-high resolution mass spectrometry study, Environ. Chem., 9, 298–319, https://doi.org/10.1071/en12016, 2012.

Riva, M., Tomaz, S., Cui, T., Lin, Y.-H., Perraudin, E., Gold, A., Stone, E. A., Villenave, E., and Surratt, J. D.: Evidence for an unrecognized secondary anthropogenic source of organosulfates and sulfonates: gas-phase oxidation of polycyclic aromatic hydrocarbons in the presence of sulfate aerosol, Environ. Sci. Technol., 49, 6654–6664, https://doi.org/10.1021/acs.est.5b00836, 2015.

Riva, M., Budisulistiorini, S. H., Zhang, Z. F., Gold, A., and Surratt, J. D.: Chemical characterization of secondary organic aerosol constituents from isoprene ozonolysis in the presence of acidic aerosol, Atmos. Environ., 130, 5–13, https://doi.org/10.1016/j.atmosenv.2015.06.027, 2016a.

Riva, M., Da Silva Barbosa, T., Lin, Y.-H., Stone, E. A., Gold, A., and Surratt, J. D.: Chemical characterization of organosulfates in secondary organic aerosol derived from the photooxidation of alkanes, Atmos. Chem. Phys., 16, 11001–11018, https://doi.org/10.5194/acp-16-11001-2016, 2016b.

Schindelka, J., Iinuma, Y., Hoffmann, D., and Herrmann, H.: Sulfate radical-initiated formation of isoprene-derived organosulfates in atmospheric aerosols, Faraday Discuss., 165, 237–259, https://doi.org/10.1039/c3fd00042g, 2013.

Shang, J., Passananti, M., Dupart, Y., Ciuraru, R., Tinel, L., Rossignol, S., Perrie, S., Zhu, T., and George, C.: SO_2 Uptake on Oleic Acid: A New Formation Pathway of Organosulfur Compounds in the Atmosphere, Environ. Sci. Tech. Let., 3, 67–72, https://doi.org/10.1021/acs.estlett.6b00006, 2016.

Shiraiwa, M., Ammann, M., Koop, T., and Poschl, U.: Gas uptake and chemical aging of semisolid organic aerosol

particles, Proc. Natl. Acad. Sci., 108, 11003–11008, https://doi.org/10.1073/pnas.1103045108, 2011.

Song, J., Li, M., Jiang, B., Wei, S., Fan, X., and Peng, P.: Molecular Characterization of Water-Soluble Humic like Substances in Smoke Particles Emitted from Combustion of Biomass Materials and Coal Using Ultrahigh-Resolution Electrospray Ionization Fourier Transform Ion Cyclotron Resonance Mass Spectrometry, Environ. Sci. Technol., 52, 2575–2585, https://doi.org/10.1021/acs.est.7b06126, 2018a.

Song, S., Gao, M., Xu, W., Shao, J., Shi, G., Wang, S., Wang, Y., Sun, Y., and McElroy, M. B.: Fine-particle pH for Beijing winter haze as inferred from different thermodynamic equilibrium models, Atmos. Chem. Phys., 18, 7423–7438, https://doi.org/10.5194/acp-18-7423-2018, 2018b.

Surratt, J. D., Gomez-Gonzalez, Y., Chan, A. W. H., Vermeylen, R., Shahgholi, M., Kleindienst, T. E., Edney, E. O., Offenberg, J. H., Lewandowski, M., Jaoui, M., Maenhaut, W., Claeys, M., Flagan, R. C., and Seinfeld, J. H.: Organosulfate formation in biogenic secondary organic aerosol, J. Phys. Chem. A, 112, 8345–8378, https://doi.org/10.1021/jp802310p, 2008.

Surratt, J. D., Chan, A. W. H., Eddingsaas, N. C., Chan, M., Loza, C. L., Kwan, A. J., Hersey, S. P., Flagan, R. C., Wennberg, P. O., and Seinfeld, J. H.: Reactive intermediates revealed in secondary organic aerosol formation from isoprene, Proc. Natl. Acad. Sci., 107, 6640–6645, https://doi.org/10.1073/pnas.0911114107, 2010.

Tang, J., Li, J., Su, T., Han, Y., Mo, Y., Jiang, H., Cui, M., Jiang, B., Chen, Y., Tang, J., Song, J., Peng, P., and Zhang, G.: Molecular compositions and optical properties of dissolved brown carbon in biomass burning, coal combustion, and vehicle emission aerosols illuminated by excitation–emission matrix spectroscopy and Fourier transform ion cyclotron resonance mass spectrometry analysis, Atmos. Chem. Phys., 20, 2513–2532, https://doi.org/10.5194/acp-20-2513-2020, 2020.

Tao, S., Lu, X., Levac, N., Bateman, A. P., Nguyen, T. B., Bones, D. L., Nizkorodov, S. A., Laskin, J., Laskin, A., and Yang, X.: Molecular characterization of organosulfates in organic aerosols from Shanghai and Los Angeles urban areas by nanospray-desorption electrospray ionization high-resolution mass spectrometry, Environ. Sci. Technol., 48, 10993–11001, https://doi.org/10.1021/es5024674, 2014.

Thomas, A. E., Glicker, H. S., Guenther, A. B., Seco, R., Vega Bustillos, O., Tota, J., Souza, R. A. F., and Smith, J. N.: Seasonal investigation of ultrafine-particle organic composition in an eastern Amazonian rainforest, Atmos. Chem. Phys., 25, 959–977, https://doi.org/10.5194/acp-25-959-2025, 2025.

Tolocka, M. P. and Turpin, B.: Contribution of organosulfur compounds to organic aerosol mass, Environ. Sci. Technol., 46, 7978–7983, https://doi.org/10.1021/es300651v, 2012.

Tong, H., Kourtchev, I., Pant, P., Keyte, I. J., O'Connor, I. P., Wenger, J. C., Pope, F. D., Harrison, R. M., and Kalberer, M.: Molecular composition of organic aerosols at urban background and road tunnel sites using ultra-high resolution mass spectrometry, Faraday Discuss., 189, 51–68, https://doi.org/10.1039/c5fd00206k, 2016.

Turpin, B. J. and Lim, H. J.: Species contributions to $PM_{2.5}$ mass concentrations: revisiting common assumptions for estimating organic mass, Aerosol Sci. Tech., 35, 602–610, https://doi.org/10.1080/02786820152051454, 2001.

Wang, D., Shen, Z., Yang, X., Huang, S., Luo, Y., Bai, G., and Cao, J.: Insight into the Role of NH_3 / NH_4^+ and NO_x / NO_3^- in the Formation of Nitrogen-Containing Brown Carbon in Chinese Megacities, Environ. Sci. Technol., 58, 4281–4290, https://doi.org/10.1021/acs.est.3c10374, 2024a.

Wang, H., Chen, X., Lu, K., Hu, R., Li, Z., Wang, H., Ma, X., Yang, X., Chen, S., Dong, H., Liu, Y., Fang, X., Zeng, L., Hu, M., and Zhang, Y.: NO_3 and N_2O_5 chemistry at a suburban site during the EXPLORE-YRD campaign in 2018, Atmos. Environ., 224, 117180, https://doi.org/10.1016/j.atmosenv.2019.117180, 2020a.

Wang, K., Zhang, Y., Huang, R.-J., Cao, J., and Hoffman, T.: UHPLC-Orbitrap mass spectrometric characterization of organic aerosol from a central European city (Mainz, Germany) and a Chinese megacity (Beijing), Atmos. Environ., 189, 22–29, https://doi.org/10.1016/j.atmosenv.2018.06.036, 2018a.

Wang, K., Zhang, Y., Huang, R. J., Wang, M., Ni, H., Kampf, C. J., Cheng, Y., Bilde, M., Glasius, M., and Hoffmann, T.: Molecular Characterization and Source Identification of Atmospheric Particulate Organosulfates Using Ultrahigh Resolution Mass Spectrometry, Environ. Sci. Technol., 53, 6192–6202, https://doi.org/10.1021/acs.est.9b02628, 2019.

Wang, K., Huang, R.-J., Brüggemann, M., Zhang, Y., Yang, L., Ni, H., Guo, J., Wang, M., Han, J., Bilde, M., Glasius, M., and Hoffmann, T.: Urban organic aerosol composition in eastern China differs from north to south: molecular insight from a liquid chromatography–mass spectrometry (Orbitrap) study, Atmos. Chem. Phys., 21, 9089–9104, https://doi.org/10.5194/acp-21-9089-2021, 2021a.

Wang, K., Zhang, Y., Tong, H., Han, J., Fu, P., Huang, R.-J., Zhang, H., and Hoffmann, T.: Molecular-Level Insights into the Relationship between Volatility of Organic Aerosol Constituents and PM2.5 Air Pollution Levels: A Study with Ultrahigh-Resolution Mass Spectrometry, Environ. Sci. Technol., https://doi.org/10.1021/acs.est.3c10662, 2024b.

Wang, X., Hayeck, N., Brueggemann, M., Yao, L., Chen, H., Zhang, C., Emmelin, C., Chen, J., George, C., and Wang, L.: Chemical characteristics of organic aerosols in shanghai: a study by ultrahigh-performance liquid chromatography coupled with Orbitrap mass spectrometry, J. Geophys. Res.-Atmos., 122, 11703–11722, https://doi.org/10.1002/2017jd026930, 2017.

Wang, X. K., Rossignol, S., Ma, Y., Yao, L., Wang, M. Y., Chen, J. M., George, C., and Wang, L.: Molecular characterization of atmospheric particulate organosulfates in three megacities at the middle and lower reaches of the Yangtze River, Atmos. Chem. Phys., 16, 2285–2298, https://doi.org/10.5194/acp-16-2285-2016, 2016.

Wang, Y., Hu, M., Guo, S., Wang, Y., Zheng, J., Yang, Y., Zhu, W., Tang, R., Li, X., Liu, Y., Le Breton, M., Du, Z., Shang, D., Wu, Y., Wu, Z., Song, Y., Lou, S., Hallquist, M., and Yu, J.: The secondary formation of organosulfates under interactions between biogenic emissions and anthropogenic pollutants in summer in Beijing, Atmos. Chem. Phys., 18, 10693–10713, https://doi.org/10.5194/acp-18-10693-2018, 2018b.

Wang, Y., Hu, M., Wang, Y.-C., Li, X., Fang, X., Tang, R., Lu, S., Wu, Y., Guo, S., Wu, Z., Hallquist, M., and Yu, J. Z.: Comparative Study of Particulate Organosulfates in Contrasting Atmospheric Environments: Field Evidence for the Significant Influence of Anthropogenic Sulfate and NO_x, Environ. Sci. Tech.

Let., 7, 787–794, https://doi.org/10.1021/acs.estlett.0c00550, 2020b.

Wang, Y., Zhao, Y., Wang, Y., Yu, J.-Z., Shao, J., Liu, P., Zhu, W., Cheng, Z., Li, Z., Yan, N., and Xiao, H.: Organosulfates in atmospheric aerosols in Shanghai, China: seasonal and interannual variability, origin, and formation mechanisms, Atmos. Chem. Phys., 21, 2959–2980, https://doi.org/10.5194/acp-21-2959-2021, 2021b.

Wang, Y., Takeuchi, M., Wang, S., Nizkorodov, S. A., France, S., Eris, G., and Ng, N. L.: Photolysis of Gas-Phase Atmospherically Relevant Monoterpene-Derived Organic Nitrates, J. Phys. Chem. A, 127, 987–999, https://doi.org/10.1021/acs.jpca.2c04307, 2023.

Weber, R. J., Guo, H., Russell, A. G., and Nenes, A.: High aerosol acidity despite declining atmospheric sulfate concentrations over the past 15 years, Nat. Geosci., 9, 282–285, https://doi.org/10.1038/ngeo2665, 2016.

Willoughby, A. S., Wozniak, A. S., and Hatcher, P. G.: A molecular-level approach for characterizing water-insoluble components of ambient organic aerosol particulates using ultrahigh-resolution mass spectrometry, Atmos. Chem. Phys., 14, 10299–10314, https://doi.org/10.5194/acp-14-10299-2014, 2014.

Wu, X., Kong, Q., Lan, Y., Sng, J., and Yu, L. E.: Refined Sea Salt Markers for Coastal Cities Facilitating Quantification of Aerosol Aging and PM2.5 Apportionment, Environ. Sci. Technol., 58, 8432–8443, https://doi.org/10.1021/acs.est.3c10142, 2024.

Xie, Q., Su, S., Chen, J., Dai, Y., Yue, S., Su, H., Tong, H., Zhao, W., Ren, L., Xu, Y., Cao, D., Li, Y., Sun, Y., Wang, Z., Liu, C.-Q., Kawamura, K., Jiang, G., Cheng, Y., and Fu, P.: Increase of nitrooxy organosulfates in firework-related urban aerosols during Chinese New Year's Eve, Atmos. Chem. Phys., 21, 11453–11465, https://doi.org/10.5194/acp-21-11453-2021, 2021.

Xie, Q. R., Li, Y., Yue, S. Y., Su, S. H., Cao, D., Xu, Y. S., Chen, J., Tong, H. J., Su, H., Cheng, Y. F., Zhao, W. Y., Hu, W., Wang, Z., Yang, T., Pan, X. L., Sun, Y. L., Wang, Z. F., Liu, C. Q., Kawamura, K., Jiang, G. B., Shiraiwa, M., and Fu, P. Q.: Increase of High Molecular Weight Organosulfate With Intensifying Urban Air Pollution in the Megacity Beijing, J. Geophys. Res.-Atmos., 125, https://doi.org/10.1029/2019JD032200, 2020.

Xing, L., Fu, T.-M., Cao, J. J., Lee, S. C., Wang, G. H., Ho, K. F., Cheng, M.-C., You, C.-F., and Wang, T. J.: Seasonal and spatial variability of the OM / OC mass ratios and high regional correlation between oxalic acid and zinc in Chinese urban organic aerosols, Atmos. Chem. Phys., 13, 4307–4318, https://doi.org/10.5194/acp-13-4307-2013, 2013.

Xu, L., Guo, H., Boyd, C. M., Klein, M., Bougiatioti, A., Cerully, K. M., Hite, J. R., Isaacman-VanWertz, G., Kreisberg, N. M., Knote, C., Olson, K., Koss, A., Goldstein, A. H., Hering, S. V., de Gouw, J., Baumann, K., Lee, S.-H., Nenes, A., Weber, R. J., and Ng, N. L.: Effects of anthropogenic emissions on aerosol formation from isoprene and monoterpenes in the southeastern United States, Proc. Natl. Acad. Sci., 112, E4509–E4509, https://doi.org/10.1073/pnas.1512279112, 2015.

Yang, T., Xu, Y., Ye, Q., Ma, Y.-J., Wang, Y.-C., Yu, J.-Z., Duan, Y.-S., Li, C.-X., Xiao, H.-W., Li, Z.-Y., Zhao, Y., and Xiao, H.-Y.: Spatial and diurnal variations of aerosol organosulfates in summertime Shanghai, China: potential influence of photochemical processes and anthropogenic sulfate pollution, Atmos. Chem. Phys., 23, 13433–13450, https://doi.org/10.5194/acp-23-13433-2023, 2023.

Yang, T., Xu, Y., Ma, Y.-J., Wang, Y.-C., Yu, J. Z., Sun, Q.-B., Xiao, H.-W., Xiao, H.-Y., and Liu, C.-Q.: Field Evidence for Constraints of Nearly Dry and Weakly Acidic Aerosol Conditions on the Formation of Organosulfates, Environ. Sci. Tech. Let., https://doi.org/10.1021/acs.estlett.4c00522, 2024.

Yang, T., Xu, Y., Wang, Y.-C., Ma, Y.-J., Xiao, H.-W., Xiao, H., and Xiao, H.-Y.: Non-biogenic sources are an important but overlooked contributor to aerosol isoprene-derived organosulfates during winter in northern China, Atmos. Chem. Phys., 25, 2967–2978, https://doi.org/10.5194/acp-25-2967-2025, 2025.

Yao, M., Zhao, Y., Hu, M., Huang, D., Wang, Y., Yu, J. Z., and Yan, N.: Multiphase Reactions between Secondary Organic Aerosol and Sulfur Dioxide: Kinetics and Contributions to Sulfate Formation and Aerosol Aging, Environ. Sci. Tech. Let., 6, 768–774, https://doi.org/10.1021/acs.estlett.9b00657, 2019.

Yao, X., Fang, M., and Chan, C. K.: The size dependence of chloride depletion in fine and coarse sea-salt particles, Atmos. Environ., 37, 743–751, https://doi.org/10.1016/S1352-2310(02)00955-X, 2003.

Yassine, M. M., Harir, M., Dabek-Zlotorzynska, E., and Schmitt-Kopplin, P.: Structural characterization of organic aerosol using Fourier transform ion cyclotron resonance mass spectrometry: aromaticity equivalent approach, Rapid Commun. Mass Spectrom., 28, 2445–2454, https://doi.org/10.1002/rcm.7038, 2014.

Ye, J., Abbatt, J. P. D., and Chan, A. W. H.: Novel pathway of SO_2 oxidation in the atmosphere: reactions with monoterpene ozonolysis intermediates and secondary organic aerosol, Atmos. Chem. Phys., 18, 5549–5565, https://doi.org/10.5194/acp-18-5549-2018, 2018.

Yee, L. D., Craven, J. S., Loza, C. L., Schilling, K. A., Ng, N. L., Canagaratna, M. R., Ziemann, P. J., Flagan, R. C., and Seinfeld, J. H.: Effect of chemical structure on secondary organic aerosol formation from C_{12} alkanes, Atmos. Chem. Phys., 13, 11121–11140, https://doi.org/10.5194/acp-13-11121-2013, 2013.

Zhang, M., Cai, D., Lin, J., Liu, Z., Li, M., Wang, Y., and Chen, J.: Molecular characterization of atmospheric organic aerosols in typical megacities in China, npj Clim. Atmos. Sci., 7, 230, https://doi.org/10.1038/s41612-024-00784-1, 2024.

Zhang, X., Li, L., Lin, Y., Wang, R., Zhu, C., Xiao, S., Cao, J., and Han, Y.: Chemical Diversity of Organosulfur Species in Various Atmospheric Environments Over the Guanzhong Basin of Northwest China, J. Geophys. Res.-Atmos., 130, https://doi.org/10.1029/2024JD042478, 2025.

Zhao, X., Hu, Q., Wang, X., Ding, X., He, Q., Zhang, Z., Shen, R., Lü, S., Liu, T., Fu, X., and Chen, L.: Composition profiles of organic aerosols from Chinese residential cooking: case study in urban Guangzhou, south China, J. Atmos. Chem., 72, 1–18, https://doi.org/10.1007/s10874-015-9298-0, 2015.

Zhu, M., Jiang, B., Li, S., Yu, Q., Yu, X., Zhang, Y., Bi, X., Yu, J., George, C., Yu, Z., and Wang, X.: Organosulfur Compounds Formed from Heterogeneous Reaction between SO_2 and Particulate-Bound Unsaturated Fatty Acids in Ambient Air, Environ. Sci. Tech. Let., 6, 318–322, https://doi.org/10.1021/acs.estlett.9b00218, 2019.